Journal Pre-proofs

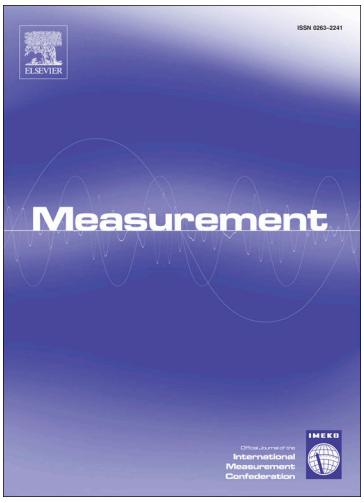

Application Of CombinedTerrestrial Laser Scanning And Unmanned Aerial Vehicle Digital Photogrammetry Method In High Rock Slope Stability Analysis: A CASE Study

Afiqah Ismail, Ahmad Safuan A Rashid, Radzuan Sa'ari, Abd Wahid Rasib, Mushairry Mustaffar, Rini Asnida Abdullah, Azman Kassim, Norbazlan Mohd Yusof, Norisam Abd Rahaman, Roohollah Kalatehjari

PII: S0263-2241(22)00418-3
DOI: https://doi.org/10.1016/j.measurement.2022.111161
Reference: MEASUR 111161

To appear in: *Measurement*

Received Date: 31 December 2021
Revised Date: 31 March 2022
Accepted Date: 3 April 2022

Please cite this article as: A. Ismail, A. Safuan A Rashid, R. Sa'ari, A. Wahid Rasib, M. Mustaffar, R. Asnida Abdullah, A. Kassim, N. Mohd Yusof, N. Abd Rahaman, R. Kalatehjari, Application Of CombinedTerrestrial Laser Scanning And Unmanned Aerial Vehicle Digital Photogrammetry Method In High Rock Slope Stability Analysis: A CASE Study, *Measurement* (2022), doi: https://doi.org/10.1016/j.measurement.2022.111161

APPLICATION OF COMBINED TERRESTRIAL LASER SCANNING AND UNMANNED AERIAL VEHICLE DIGITAL PHOTOGRAMMETRY METHOD IN HIGH ROCK SLOPE STABILITY ANALYSIS: A CASE STUDY

Afiqah Ismail[1], Ahmad Safuan A Rashid[1,2], Radzuan Sa'ari[1], Abd Wahid Rasib[3], Mushairry Mustaffar[1], Rini Asnida Abdullah[1], Azman Kassim[1], Norbazlan Mohd Yusof [4], Norisam Abd Rahaman[4], Roohollah Kalatehjari[5]

[1]School of Civil Engineering, Universiti Teknologi Malaysia, 81310, Johor Bahru, Johor. afiqahismail912@gmail.com;ahmadsafuan@utm.my; radzuans@utm.my; mushairry@utm.my; asnida@utm.my; azmankassim@utm.my

[2]Centre of Tropical Geoengineering, School of Civil Engineering, Universiti Teknologi Malaysia, 81310, Johor Bahru, Johor.

[3]Faculty of Built Environment and Survey, Universiti Teknologi Malaysia, 81310, Johor Bahru, Johor. abdwahid@utm.my

[4]Persada PLUS, KM15, Lebuhraya Baru Lembah Klang, Persimpangan Bertingkat Subang, Selangor, 47301 Petaling Jaya, Selangor. bazlan@plus.uemnet.com; norisam@plus.uemnet.com.

[5]Department of Built Environment Engineering, School of Future Environments, Auckland University of Technology, Auckland 1010, New Zealand. r.kalatehjari@aut.ac.nz.

APPLICATION OF COMBINED TERRESTRIAL LASER SCANNING AND UNMANNED AERIAL VEHICLE DIGITAL PHOTOGRAMMETRY METHOD IN HIGH ROCK SLOPE STABILITY ANALYSIS: A CASE STUDY

Abstract

Recent advancements in remote sensing techniques have made it possible to overcome the risky issues using conventional methods and have opened up new opportunities for collecting data on discontinuity characteristics. This research compares the application of a Terrestrial Laser Scanner (TLS) and Unmanned Aerial Vehicle (UAV) in rock slope stability analysis. Two case studies, Ulu Choh Quarry and Jelapang Rock Slope are analysed using Kinematic Analysis and Slope Mass Rating (SMR) to depict rock through the 3D point cloud. The techniques are compared with the hand mapping method concerning the accuracy of the data acquisition in assessing the rock slope. The standard deviation for the dip and dip direction between digital capture and hand mapping is 2.97° and 2.86°, which falls under the acceptable tolerance limit. The integration of UAV and TLS also generates excellent clear point cloud data from the top to the toe of the slope.

Keywords: Rock Slope Stability; 3D point cloud; Discontinuity extraction; Terrestrial Laser Scanner; Unmanned Aerial Vehicle.

1. Introduction

There has been an increase in the development of rock slopes for the reconstruction of roads, tunnels, and highways. Construction involves excavations and cuttings in the original high rock slopes. According to Ji and Liao (2014), natural terrain will be interrupted due to infrastructure buildout and extensive engineering projects. Problems arise when the rock slope is bound to a

fault, and a weak plane problem leads to slope failure. The impact of a failure on high rock slopes can result in serious accidents, injury, and economic losses. Smith and Arnhardt (2016) observed that rock joints control different types of failure: planar sliding, wedge sliding, toppling, or circular failure. The stabilisation of rock slopes is strongly influenced by the orientation and number of structural characteristics, such as faults, folds, and joints (Stead & Walter, 2015). Thus, it is necessary to monitor the rock slope and predict the level of stability of the slope. Knowledge and assessment of the processes that control slope behaviour (in slope stability analysis) are needed to avoid failure. Over the years, researchers have always found a way to characterise rock mass in terms of the colour, presence of cracks, moisture, etc., to obtain the best and ideal prediction of the rock slope stability.

An appropriate and targeted prediction model is key to a rock slope stability assessment. There are several methods available to assess rock slope stability. Slope Mass Rating (Romana, 1985) is one of the most used classification systems which focusses on the condition of the rock mass properties. Romana et al. (2013) provided a thirty-year evaluation of the SMR system, emphasising the system's advantages and advancements. This technique required information about the strength parameters, discontinuity length, weathering grade, etc. SMR slope stability is analysed by first rating the properties. Detail description of geometrical parameters in computed SMR is discussed in Pastor et al. (2019). Site geologists are still implementing conventional geological mapping methods by hand mapping and walkover survey methods to obtain the crucial geological parameters for rating the SMR. The orientation of discontinuities (dip/strike), number of joint sets, and other relevant geological data are collected in the journal when the geologist walks across the site during geological survey mapping.

However this method has several drawbacks, including accessibility difficulties to the site, the limitations of the use of traditional tools to evaluate the characteristics of large areas, and restrictions on the identification and localisation of site features (Matasci et al., 2015; Tan et al., 2015). Furthermore, geological mapping can be dangerous and life-threatening for the person managing the site, especially in areas with steep and elevated rocky slopes, because this method requires physical contact with the slope. Frayssines and Hantz (2006) also commented on points of weakness in this rating technique, such as the person in charge is vulnerable to risk while collecting the data, inconsistencies can occur because of subjective measurements, and the view of a person in charge influences it, data can usually be obtained in the accessible areas (such as the toe of the slope), but data from the upper part of the slope is not being taken. In addition, the exact location of the failure that may occur cannot be identified through the rating system. Feng (2012) also emphasised that geological survey mapping takes a long time to complete as the whole study area needs to be covered during fieldwork, followed by laboratory testing and analysis.

Therefore, there is a need for an alternative method that can eliminate the discussed drawbacks of conventional geological mapping methods. This workflow can be enhanced and be more effective if geological data is digitally identified and captured in the field (Schlatter et al., 2010). Detailed mapping of geological features can be obtained by capturing high-resolution data from the rock slope point cloud. This will also allow for digital analysis of the geological features. In addition, this method is useful for data collection when human access to the site is limited. Based on Lato and Vöge (2012) and Westen et al. (2008), the advancement of remote sensing (e.g., digital photogrammetry) benefits rock stability assessment as it represents the slope with good resolution and accuracy of the 3D point cloud. Long et al. (2021) and Rasmussen (2020) recently has applied the methods to identify rock blocks and calculate the

size of the block automatically through the point cloud. This technique can prevent workers from being exposed to risks during the fieldwork. To obtain their kinematic analysis, important structural features can be extracted from Light Detection and Ranging (LiDar) (Lato et al., 2009; Oppikofer et al., 2009; Sturzenegger & Stead, 2009).

The accessibility of state-of-the-art remote sensing technologies (mainly concentrated in satellite, aerial, and terrestrial platforms) grants comprehensive and up-to-date data collection over a wide area. Therefore, it could improve the production of a 3-dimensional (3D) model of the rock slope with reduced costs and optimised fieldwork (Guzezeti et al., 2012; Frodella et al., 2017). Due to technological advancements, there has been a big change in mapping 2-dimensional to 3-dimensional models over the last ten years (Chen et al., 2021; Li et al., 2022). Azarafza et al. (2017) have developed an algorithm to model the structural geology within a rock mass in 3D space, and it contains detailed information on the discontinuity. Other than that, Chanut et al. (2021) and Liu et al. (2021) used a method of studying the evolution of landslides based on a multi-date point cloud over time. This method can improve the minimum displacement value that can be detected. Mazzanti et al. (2021) have also been able to analyse the geomorphological evolution of a scarp from 2016 until the present by using the 3D model of the scarp. There are many kinds of remote sensing techniques that are used to monitor rock slopes: Ground-Based Synthetic Aperture Radar Interferometry (GB-InSAR), Terrestrial Laser Scanning (TLS), Unmanned Aerial Vehicles (UAV), and Terrestrial Optical Photogrammetry (TOP). **Table 1** presents the advantages and disadvantages of the different techniques.

Digital Photogrammetry and Terrestrial Laser Scanner (TLS) are among the latest and most used methods to obtain a 3D model of a rock mass (Di Crescenzo & Santo, 2007; Ferrero et al., 2011; Jaboyedoff et al., 2012; Frohlych & Mettenleiter, 2004). Recently, UAV and TLS

were applied by Zhou et al. (2020) to calculate the volume of the failed mass at the Schuiceng Landslide. The scale of the site, its geographical location (e.g., coastal, mountainous, or urbanised area), rock mass morphology, and the degree of detail required is essential information in the method selection process. An unmanned aerial vehicle (UAV) allows remote data acquisition in vertical or horizontal stripes. UAV could cross a distance of a few tens of metres from the rock face and, therefore, increase the measurement details of the discontinuities and the slope surface (Danzi et al., 2013). On the other hand, the main advantages of TLS are its ability to specify and detect rock types from a distance accurately, accumulate a large number of measurements in inaccessible vertical areas, and perform fast and accurate data collection over broad areas (Abellán et al., 2014). This enables large 3D models of geological bodies to be built more productively and increases the possibilities for the dynamic 3D visualisation of geological features.

The discontinuity features collected from 3 dimensional point cloud acquired from TLS and UAV data are used in this case study. In this study, two different techniques, TLS and UAV, were used at two different locations. The TLS was applied at the Ulu Choh Quarry to produce the 3D image of the rock slope. On the other hand, TLS was also used with a UAV at the Jelapang Rock Slope. During the rock slope assessment, the kinematic analysis method was used, which involves stereographic projection principles. This method has been found to be useful in the stability assessment process as well as a preliminary indicator of the risk of slope failure. Besides this, the Slope Mass Rating index was reviewed through the 3D point cloud data, as the source of information. This paper comprises i) the background of the study, ii) an explanation of the methodology used, and iii) a discussion on the results and analysis obtained from both applications. The reliability and 'pros and cons' of TLS and UAV are also discussed in this paper.

2. Background of the study

2.1 Brief Introduction of Two Case Studies

This section will explain the details of the two different case studies that have been chosen to operate the suggested methodology. The UAV and TLS were used to assess the rock slope quality through kinematic analysis and Slope Mass Rating.

2.1.1 Case Study 1: Ulu Choh Quarry, Johor

The first study aimed to identify the dip and dip direction of the joints from TLS and then to validate the ground observations by using a geological compass at Ulu Choh Quarry, Johor. Kinematic analysis and Slope Mass Rating assessment were also undertaken. The case study focused on a rock quarry owned by Malaysian Rock Products Sdn Bhd (IJM) in Ulu Choh, Johor (**Figure 1**). The rock slope is located in the Western Belt of Peninsular Malaysia at latitude 1.537666 and longitude 103.546389. The general geology of the area is comprised of acidic rock, notably medium-grained leucogranite, and there is a range of weathering classes, from fresh to highly weathered granite, according to the geological map prepared by Geosains (2012). Despite this, the study focused on a small area of the quarry (100 m in width and 50 m in height), and the weathering grade of the target region was fresh to slightly weathered (III) granite (Ismail et al., 2020). Natural and man-made joints in the rock slope were observed due to the quarry's blasting activities.

2.1.2 Case Study 2: Jelapang Rock Slope

The purpose of the second case study was to measure the SMR of the slope by using a combination of two surveying techniques: UAV and TLS. The basic Rock Mass Rating (RMR) details, such as weathering, roughness, infilling, persistence, and aperture, were obtained from the fieldwork and the 3D point cloud. The study area was in Perak state, part of the Western

Belt of Peninsular Malaysia, along the North-South Expressway between Ipoh and Kuala Kangsar, with coordinates 4.692147, 101.016301 (as illustrated in **Figures 2 and 3)**. The slope is an approximately 800 m long, bulging rock slope with the highest peak of around 120 m above ground level. This rock slope is heavily fractured and steep and is sited in the Northeast-Southwest Kledang Range, a massive granitic pluton. With that being said, the stability of this rock slope must be adequately considered and monitored as it will affect the safety of expressway users.

2.2 Terrestrial Laser Scanner (TLS)

TLS was used to acquire the 3D point cloud of the Ulu Choh rock slope. The TLS was used for structural mapping of the rock slope surface by providing a high-density point cloud to determine the rock surface geology parameters, such as geological orientation and dip and dip direction. The slope stability analysis was carried out using the Slope Mass Rating (SMR) method from the data collected. Discussions in this section cover the surveying instrumentation, the Ground Control Points (GCPs) survey using Real-Time Kinematic (RTK) and Global Positioning System (GPS), TLS data acquisition, TLS point cloud data processing, and TLS point cloud 3D modelling.

2.2.1 Surveying Instruments and Software

Table 2 shows the surveying instruments used at Ulu Choh Quarry. South Galaxy 1 (Based & Rover) units were used to establish TLS GCPS. The GPS observation technique used is an RTK GPS technique with an accuracy of ±1cm and ±2cm in the horizontal and vertical, respectively. At the same time, two units of Topcon Hyper II receivers were used for the static survey. Two reference control points were established with a post-processed model. **Table 3** shows the Topcon Magnet Tools and Scan Master Software was used to process GPS static

observations and generate a point cloud. All TLS GCPs spatial coordinates were referred to as MRSO GDM2000 coordinate systems.

2.2.2 Real-Time Kinematic Global Positioning System (RTK GPS) Survey to Establish Ground Control Points (GCPs)

Virtual Reference Station (VRS) in MyRTKnet infrastructure initiated two reference stations by using static observation post-processed mode. It tooks about half an hour for every station to be observed. Topcon Magnet Tools was used to process the GPS static observations. All TLS GCPs spatial coordinates were referred to as MRSO GDM2000 coordinate systems. While the TLS rock slope mapping was controlled using GCPs established throughout the survey area, the positions of these GCPs were established using a Real-Time Kinematic Global Positioning System (RTK GPS). A GPS receiver that acts as the BASE was on a point with known coordinates. The BASE receiver was corrected up to 1 – 2 km (using internal UHF radio) to the receiver (known as a ROVER) placed on the GCPs. This study used two sets of RTK GPS (Based and Rover), namely Topcon Hyper II and South Galaxy 1. The RTK GPS positioning accuracies were within centimetre levels.

3.1.3 Data Acquisition

Analysing the reflection of laser light on the object's surface and determining the distance to an object is a remote sensing method called Terrestrial Laser Scanning (Takashi et al., 2011; Walsh et al., 2018). The TLS end product is a 3D point cloud in which the image that has been captured is presented in the form of millions (XYZ) of points with their relative position to the target surfaces. Topcon GLS 2000 is the TLS model that was applied in this study, and this equipment is measured according to the time of flight (TOF). The time pulse method is another name for TOF. The TOF method measures the time between the emission of the signal, the

reflection by the object, and its return to the sensor (**Figure 4**). The object's distance can be calculated using the formula D = t/v, where D is the slope distance, v is the speed of electromagnetic radiation and t is the measured time of travelling or time of flight (Zam et al., 2018). A detailed study of TOF laser range determination can be found in Reshetyuk (2006) and Grönwal et al. (2017). For case study 1, a fast-moving rapid mode at 12 mm and a distance of 10 m from the rock slope were recorded using TLS to obtain the point cloud density. Five megapixels of the resolution were used in the TLS internal camera to record and scan the panoramic image shown in **Figure 5**. The TLS memory was used to store all information, including the setting parameters used, occupied station, the backsight target, the scanned point cloud, and the scanned images. The TLS points cloud was subsequently aligned by using a geodetic Global Positioning System (GPS) receiver to determine the position of TLS CGPs. This operation is required in order to georeference the point cloud on a chosen reference coordinate system and merge two or more scans of the same object, realised from different points of view.

Terrestrial Field Data Collection was also carried out in case study 2. The technique of TLS that was carried out at the quarry was also undertaken at accessible areas along the highway. A total number of 38 scans were established using the TLS (**Figure 6**). Specially designed strawboard holders were planted on the surface of the outcrop using a Topcon GLS-2000 laser scanner. Besides that, the prism was also used as a target scan in this research and placed on the control point. Upon completion of TLS field data acquisition, the following data (occupied station information, backsight station information, instrument height, the height of the backsight target, digital images of the scan area, scan point clouds, and scanning setting parameters) were stored in one job. The job folder name was based on the TLS occupied station. All job folders were then transferred to a PC for data processing using ScanMaster software.

2.3 Unmanned Aerial Vehicle (UAV)

A DJI Phantom 4 Pro drone, mounted with a 20 megapixel camera, was used as a UAV to capture images of the rock slope. Reference points were created to allow the drone to capture pictures to cover the required region, and a total of one hundred images were taken from the top and side views of the rock slope. Agisoft PhotoScan Professional software was used to process the imagery. The software runs through a Structure from Motion (SfM) algorithm, which detects features in the image for bundle adjustment. The SfM photogrammetric method uses overlapping images to create three-dimensional surface models (Agisoft, 2016). Ground controls were also implemented on-site to ensure that the photogrammetry process generated accurate and reliable results. The outputs from the photogrammetry process are a 3D model, a 3D dense point cloud, an orthophoto, and a Digital Surface Model (DSM). The great versatility and the likelihood of achieving high altitudes indicate that this method can also be carried out under challenging morphological conditions. One can continuously track the survey through a monitor while simultaneously zooming along with essential points. The ability of the drone to fly very close to the slope surface allows for important geostructural observations and helps to recognise open joints parallel to the rock slop, which TLS does not readily identify.

2.3.1 Data Acquisition

The primary data involved drones and sensors from RGB, NIR, and IRT. These image data were collected through the fieldwork carried out using DJI Phantom 4 with MAPIR Survey 2 NIR and RGB sensors. The specification of the UAVs and sensors is given in **Table 4**. A multirotor UAV was used as a platform to manoeuvre and acquire the close-range remote sensing images approximately 20 m from the rock surface. Multirotor UAVs can land and take off vertically. Therefore, this type of UAV is suitable for describing a complex and steep, high outcrop in a narrow space. The defined area, the flight height, the overlapping of images, and

camera types are essential things to be set up in generating a flight plan. By following Nex and Remondino (2013), the image had to overlap about 80%, along with the waypoints that had been set up. After that, the UAV could automatically take off and fly along the tracks according to the flight plan. The images could then be captured, and the UAV landed at the home point.

2.4 Point Cloud Generation and Data Processing

All collected data were transferred to a desktop computer for data processing purposes. The raw data underwent image-stitching and layer stacking to create an orthophoto and overlay two orthophotos under a single database, respectively. This process was conducted using Pix4D Mapper Software for RGB images, and NIR was conducted using Agisoft PhotoScan Professional Software. After the stitching was carried out, the orthophoto of RGB and NIR underwent the stacking process, which overlayed two different images together to extract the value of the Normalised Difference Water Index (NDWI). RGB and NIR orthophotos were stacked together using a georeferencing function in ArcGIS ArcMap 10.3 software. The RGB orthophoto was used with the applied image-to-image geometric correction method.

Multiple scanned data from the Terrestrial Laser Scanner was registered and then georeferenced. Subsequently, various processes such as data registration, point cloud colouring, georeferencing, and data editing (cleaning/ resampling/ filtering) took place in Topcon Scan Master Software to create the 3D point cloud of the rock slope surface model. The high-density points cloud produced was then used to generate the 3D surface of the rock slope. **Figure 7** shows the model obtained by laser scanning the slope. Georeferencing enables the position of the entire dataset to the coordinates of the tie point constraints measured using GPS or total station with the coordinate from the laser scanner. All of the coordinate values of the control points and target sheets obtained from the total station were used and created in this process.

Figure 8 shows all the new points that were created that appear in the Point Folder in the Project Explorer. On completion, the created points were associated with the corresponding tie point constraints.

Data cleaning is one of the components that was processed through Scan Master software. This part was used to delete the unnecessary points from the point cloud. The data cleaning process can be done by several tools that are provided in the scan master. The polygon selection icon on the toolbar picks the unwanted scanned data and deletes it using the Delete Data icon (Zam et al., 2018). Irregular noise can also be removed by using the Filtering Noise method in Scan Master software. By adjusting the slider bar, isolated points or irregular noise were selected and then all the selected points were removed by clicking on the Delete Data icon on the toolbar. After editing, the datasets were exported in ".pts" format for processing in the Cloud Compare software. The high-density points cloud produced was then used to generate the 3D surface of the rock slope. At this stage, the point cloud data from the UAV was merged with the TLS to enhance the rock surface information (**Figure 9**).

3. Geostructural Survey

Geostructural mapping was accomplished for the rock slopes through the definition of geomechanical descriptions of the rock mass (Ferrero et al., 2007). Due to the height and huge size of the slope, the conventional method was integrated with advanced techniques to determine structural data. The methodological approach that was followed for the stability analysis is described in this section (**Figure 10**).

3.1 Conventional Compass Survey

A series of geostructural surveys along scanlines of 10 m lengths was carried out for validation. More than 70 geostructural traverses were performed with a total of about 2600 discontinuities collected in terms of orientation, spacing, persistence, roughness, and general condition (alteration, aperture, filling), in accordance with the ISRM suggested method. All of the data collected were analysed separately for every traverse, using DIPs software to identify the dominant joint set. This software can determine the clusters of the different joint sets. Observation of local instabilities, the presence of water, and structural supports were noted separately for integrating the results of the survey (**Figure 11**).

3.2 Extraction of Discontinuity from Point Cloud

The 3D image and point cloud were imported into Topcon Scan Master Software for manually delineating discontinuities by inserting measure angles or distance tools (**Figure 9**). The scanline survey method was practised through the Scan Master Software. The computer mouse was used to select a line or plane of discontinuities on the point cloud. A combination of the point cloud and image data was used to extract the discontinuity trace coordinates and to determine the discontinuity's geometric parameters and spatial location. It is important to match the point cloud coordinate system to the geodetic coordinate system at the study site in order to assess their significance (Zhang et al., 2019). The Scan Master program identified the points within the plane to calculate the dip and dip direction of the best-fit plane running through the points. The dip, dip direction, and trace length were obtained using the point coordinates along the traces for each extracted trace. The scanline survey method was practiced through the Scan Master Software on the hybrid point cloud to identify the joints from the rock slope and draw them using its 'measure angle' tool. In geology, a scanline method records important rock features and discontinuities such as joint spacing, surface roughness, aperture, and persistence that cut across a single straight line with a certain length and orientation at an exposed rock

surface (Guyer, 2017; ISRM, 1981). After detecting all the discontinuities, the data were gathered and transferred into Topcon Magnet Office Software to obtain the corrected values of joint orientation (**Figure 12**). **Figure 13** shows the principle of the joint set observed on the part of the rock slopes.

3.3 Kinematic Analysis

Kinematic analysis is a technique used to determine the propensity for rock slope failures (plane, wedge, and toppling failures) due to the presence of unfavourably oriented discontinuities. According to ISRM (1978), geological discontinuities are any mechanical rupture within rock masses, such as joints, weak bedding planes, weakness zones, and faults. The joint orientation data collected through the Topcon ScanMaster software and the results of the walkover survey (using a Brunton Compass) were used with Rocscience Dips Version 7.0 to identify the clusters of poles of discontinuity orientations (Hoek & Bray, 1981). Dips software is a graphical and statistical method used to analyse and visualise the orientation data in stereographic projection (stereonet). The visual investigation or implementation of density contours in stereonets helps to identify the clusters of poles of discontinuity orientations (Kundu et al., 2022). By choosing the slope orientation, friction angle, and lateral limits, the kinematic analysis function provides the ability to search for different rock slope stability modes in a stereonet plot (Kumar & Pandey,2021). This method is capable of identifying the critical percentage of potential rock block movement in various failure modes.

3.4 Conversion of data into Slope Mass Rating Value

The Slope Mass Rating (SMR) index system was proposed by Romana (1985). SMR is estimated by assigning a specific rating to each parameter, and it is used to understand the stability and probability of slope failure (Azarafza et al., 2017; Tomas et al.,2012). The Rock

Mass Rating (RMR) score is the basic SMR value component. By subtracting a factor based on the joint-slope relationship and adding a factor based on the excavation method, the value is adjusted (Alam and Sadique, 2021).

$$SMR = RMR + R6 \quad (1)$$

Rock mass properties are the first input parameters that refer to the Rock Mass Rating (RMR). The RMR classification system was selected as the base system due to its ease of use and good correlation with rock mass mechanical parameters (Maazallahi & Majdi, 2021). The basic RMR is the sume of individual rating and the RMR value ranges from 0 to 100 (Yellas et al., 2021). RMR is evaluated according to Beniawski's (1979) proposal.

$$RMR\ (b) = R(UCS) + R(SD) + R(CD) + R(GD) + R\ (RQD) \quad (2)$$

where UCS is the rock's uniaxial compressive strength, SD and CD are the spacing and condition of the discontinuity, respectively, GD is the groundwater inflow through the discontinuity, and RQD is the rock quality designation. All of the rock parameters are evaluated in the form of a rating by referring to the suggested method proposed by ISRM (1981) and ISRM (1985). The computation of the RMR_b is characterised by field observations (e.g., Uniaxial Compressive strength - UCS, weathering, and groundwater) and scanlines (aperture, roughness, and infilling), observations on the images (infilling), and on the 3D point cloud (RQD, spacing, persistence, and aperture). For measuring rock strength, a few samples from the outcrop were taken to the laboratory for Uniaxial Compressive Strength testing. A Schmidt Hammer was also used at the site to test the in situ strength of the intact rock. For R2, Rock Quality Designation (RQD) was obtained from digital photogrammetry. Rock Quality

Designation (RQD) is defined as the percentage of rock cores that have a length equal to or greater than 10 cm over the total scan line length (Pantaweesak, Sontamino and Tonnayopas, 2019). The exposed rock outcrop is divided into a small area of 10 m in length through point cloud measurement. An exposed discontinuity that has a length of more than 10 cm is then recorded and the data is used to calculate the RQD value, as shown in Eq. (3).

$$RQD = 115 - 3.3\ Jv \quad (3)$$

$Jv = \sum (1/S1)$

S1 = spacing of discontinuity

S1 (Joint Set 1) = 0.5 S2 (Joint Set 3) = 2

$Jv = \sum (1/0.5+1/2)$

$Jv = 2+0.33$

$RQD = 115 - 3.3\ Jv$

$RQD = 115 - 3.3\ (2.33)$

$RQD = 107.31$

Based on ISRM (1985), the RQD for region 4 falls into rating (R2) = 20.

R3 is the spacing between discontinuities, which is the distance measured perpendicular to the discontinuity planes. The discontinuity spacing can be directly measured through the Scan Master software, using the Measure Distance tool icon. On the other hand, R3 is the condition of the discontinuity. After Beniawski (1989), the condition of the discontinuity consists of:

i. Persistence: Size of discontinuity within a plane
ii. Aperture: Distance that separates the adjacent rock surface of an open discontinuity

iii. Roughness: Texture of the plane surface

iv. Infilling: Material separating the adjacent rock surfaces of discontinuities

v. Weathering: Alteration of rock due to hydrothermal process

All of the data collected were simplified in table form, as shown in **Table 5**. **Figure 14** shows the persistence of the joint, measured through the icon tool in the Scan Master software.

R6 in SMR is the orientation of the discontinuities and is calculated as:

$$R6 = (F1 \times F2 \times F3) + F4 \quad (4)$$

The discontinuity orientation is the part that needs to be considered in the SMR determination (Azarafza et al.,2021). **Table 6** shows the adjustment factors in SMR. Dip and dip direction is defined by using the stereonet dips method. Below is the critical parameter that should be derived for all regions.

$$F1 = \alpha j - \alpha S \quad (5)$$

The angle between the joint and slope face strike will define their parallelism, F1. F1 ranges from 1.00 to 0.15. If they are near to parallel, the value will be near 1.00, while if the angles are more than 30 ^{o}, the value is 0.15.

$$F2 = \beta j \quad (6)$$

In the planar mode of failure, F2 values range from 1.00 to 0.15, depending on the dip angle of the joint. If the angle is more than 45^o then the dipping of the joint is 1.00, while and angle less than 20^o is nearer to 0.15.

$$F3 = \beta j - \beta s \quad (7)$$

The scoring of F3 is determined by the correlation between slope face and joint dip. A fair condition is considered for the slope face and near to parallel joints. However, a very unfavourable situation is considered if the slope dips 10^o more than the joint. Factor F4 is the adjustment factor for the excavation method, and it has been empirically determined, as stated by Romana (1985). It ranges from -8 to 15, where -8 is selected as a poorly blasted slope while 15 if for a natural slope (Azarafza et al., 2017). Riquelme et al. (2016) stated that an initial analysis of the relative position of the joint planes and the slope (for a planar failure mechanism), along with the intersection line between two planes (for wedge failure), is compulsory when calculating the geometrical parameter defined above. The probability of failure can also be determined from the value of the Slope Mass Rating.

4. Results and Discussion

4.1 Case Study 1: 3D Model of Ulu Choh Quarry Rock Slope

Figure 15 is the rock slope model of the Ulu Choh Quarry, which was obtained through the TLS. 5,517310 point clouds were generated after photo alignment and cleaning useless point cloud data. The point cloud from TLS only covers 200 m width and 30 m heights of the rock slope. Other than that, some parts of the rock slope were missing or unclear. The missing information was hidden by some hard objects when TLS collected the data or was due to the distance of TLS to the rock slope surface. Due to the location of the broad and busy highways,

TLS could only be placed very near the slope or far from it. It might be impossible to investigate the whole area by using TLS if there is no access to a suitable surface and location on the ground.

4.1.1 Accuracy Consideration and Kinematic Analysis

In this case study, the extraction of joint orientation was carried out through two different methods, directly during the fieldwork and the second measure through the 3D point cloud. **Figure 16** shows the joints that were identified in case study 1. The joints were redrawn using the measure angle tools. Then, the data was gathered and transferred into magnet tools to obtain the orientation of the joints.

The orientation data (dip/dip direction) collected by TLS and the traditional method were compared, to determine their differences. Dip and dip direction measurements from the TLS and through the Brunton, compass method are represented in **Table 7**. Comparing these measurements shows that the results of the classical approach are similar to the TLS-derived values. There must be a tolerance or error limit between hand mapping and digital capture of less than ± 15 ^{o} (Matsimbe, 2020). For the dip, the standard deviation is 1.41^{o}, while the mean value is 2^{o}. For the dip direction, the standard deviation is 1.22^{o}, and their mean value is 3^{o}. The slight differences might be due to the low density of the point cloud. **Figure 17** shows natural joints in a 100 m linear traverse chosen from the quarry. The data was transferred onto a stereonet, using the Dips Software to compare the kinematic result, as shown in **Figure 18**. The results prove that TLS and compass data have similar values and trends. This comparison indicates that the TLS method can precisely measure discontinuity angles and directions. Based on the graphical analysis, three joint sets were identified in the area, two of which are the

prominent joint sets. Most of the major joints are dipping towards the North East, with the mean of trend value being 45^{o} and the mean dip value being 75^{o}.

4.1.2 Slope Stability Analysis of the Ulu Choh Quarry

A fast check on different modes of rock failure was performed by inserting the value of slope orientation, friction angle, and lateral limits in the kinematic analysis feature through DIPS software. The kinematic analysis results show 40% wedge sliding and 40% flexural toppling (**Figure 19**). This meant that there is a 40% chance of flexural toppling or wedge sliding if the slope fails. Hence, TLS has proven helpful as a tool in rock slope characterisation, by providing valuable preliminary information on rock slope stability.

Rock Mass properties were collected and observed through the point cloud to calculate the Rock Mass Rating (RMR), as shown in **Table 8**. The rock mass rating of the Ulu Choh Quarry is underclass II, which is consider to be Good rock. The Slope Mass Rating (SMR) for the second case study is 66, categorised as a Stable slope (**Table 9**). These results show that TLS can be used to analyse the stability of rock by both SMR and kinematic analysis. However, it requires certain conditions to obtain a clear image of the targeted area. A narrow, high, steep area might cause problems if TLS is used as a stand-alone method in the field.

4.2 Case study 2: 3D Model of Jelapang Rock Slope

Due to the limitation on coverage of the rock slope at Ulu Choh quarry by TLS, a UAV drone image was used along with TLS in Jelapang, to generate a 3D model of the Rock Slope by the image-based modelling technique. Agisoft Photoscan Professional software was used to create the point cloud from photos taken at different angles using the UAV and TLS. Photos were tied together by identifying the same set of points from two or more images. A point cloud with

7,641,725 points was generated after photo alignment and cleaning. The final 3D model was produced after the mesh and texture processing, as shown in **Figure 9**. It is shown that the location of rock discontinuities can be identified clearly, where the point cloud data was significant enough to do the measurement.

4.2.1 Accuracy Consideration and Scanline Traversing

The rock slope in Jelapang was divided into several regions (**Figure 20**), and the scan line traversing method was performed with an interval of 100 m for each region (ISRM, 1981). A direct measurement was conducted in the 3D model, to determine the capability and performance of image-based modelling for dimension measurement applications. Rock discontinuities, such as joints and faults, were identified using Topcon Scan Master software and orientation was measured using the scanline traversing method. The model analysis produced the attitude and location of the discontinuities and the number of joint sets, dip orientation, and other joint parameters were determined along the scanline. A 100 m scanline from Line 1, located at the base of the slope, was used to verify the results of the digital photogrammetrics in comparison with the Brunton compass results. The dip angle and orientation of the joints, obtained from the software, are presented in **Table 10,** and the results of the walkover survey (using the Brunton Compass) are shown in **Table 11**. For the dip, the standard deviation is 2.97^{o}, while the mean value is 4.14^{o}. For the dip direction, the standard deviation is 2.85^{o}, and their mean value is 2.9^{o}. The digitalised photogrammetry shows slightly higher dip and dip direction variation than the hand mapping method.

The failure mode can be obtained from the Dips Software by performing the graphical analysis. **Figure 21** shows the stereogram results from the analysis of a hybrid point cloud with those obtained by the walkover survey using the Brunton Compass. According to the results, the

hybrid point cloud of the TLS-UAV shows that the most critical type of failure is wedge failure, with a probability of 15.22%. Brunton Compass survey results show the same wedge failure as being the most critical failure type, with a probability of 14.10%. Considering that both analyses resulted in an identical failure type and a very close probability of failure, it is verified that the proposed digital photogrammetry method is fast and accurate in measuring the rock parameters.

4.2.2 Rock Slope Stability Analysis for Jelapang

The Rock Mass Rating (RMR basic) was estimated for every region (**Tables 12** and **13**), where most rock slope regions are categorised as rock mass Class II and Good and Stable, based on the Romano (1985) approach. Region 12 is categorised as Class III, which is Fair and Partially Stable. The SMR value was calculated for every region based on the estimated RMR values (**Table 14**). Due to the low SMR values, regions 6, 12, 13, and 14 are critical and categorised under Fair and Bad Slope Stability. They fall in Class III and IV, Partially Stable and Unstable. The inferred failure is planar (along joints) or wedge failure, but it could be a large planar and wedge failure. There is a 60% chance of wedge sliding at region 12 if the slope fails, while the likelihood of planar or wedge failure for regions 6, 13, and 14 is 40%.

The analysis identified three major joint orientations on the rock slope: South West, South East, and North East. Based on the SMR calculation, region 12 has the lowest Slope Mass Rating value (39), followed by region 13, region 14, and region 6. Region 12 is considered an unstable slope, while regions 13, 14, and 6 are categorised as partially stable slopes. The main failure types at these unstable and partially stable slopes are planar sliding and wedge failure.

4.3 Comparison between TLS and UAV

This paper discussed and delivered the results and analyses of the 3D model generated using UAV and TLS. The standalone TLS method only covers a part of the rock slope. Some parts of the rock slope are missing due to the surrounding relief and ditches and the limited field of view of the scanner, and no station was high enough to acquire the upper parts of the rock slope. Some outcrops do not show clear discontinuity patterns, so they do not identify them. A clear image is only available at the centre of the rock slope. Therefore, scanline traversing can only be done in this part of the rock slope. Integrating UAV and TLS produces a better quality point cloud as the UAV's orthophotographs can enhance the TLS point cloud. This integration also creates a full image of the broad and steep rock slope from the top to the toe of the rock slope, due to the ability of the UAV to fly in vertical and oblique ways to capture all of the required images. Comparing both TLS and UAV with the direct classical method proves their accurate acquisition of geological measurements. Using SMR through the photogrammetry model, both methods offer a more straightforward rock stability assessment than the classical method.

4.4 Benefits, Limitations, and Recommendations

In the studies conducted, the integration of UAV and TLS displays the following benefits and limitations. A recommendation for further research is also suggested.

Benefits:

1. The camera does not require direct contact with the investigated scenario, making it safe to measure hazardous areas.
2. Dip and orientation of discontinuities can be measured in Scan Master software;
3. Parameters of joint (persistence, number of joint sets, spacing) and rock mass properties can be measured through the digitalised photogrammetry.

Limitations

1. The distance range for the Terrestrial Laser Scanner is 10 m with 3.5mm point spacing accuracy (Akgul et al., 2016; Tan et al., 2018). According to Abellan et al. (2014), the accuracy of the measurement decreases with increasing range, the complexity of the scanned surface and the angle of incidence. In this study, the TLS distance range is set to be 6 m from the targeted subject while the UAV altitude is less than 10 m. RMR parameters that can be measured from the point cloud are RQD values, joint spacing (Js) and joint condition (Jc). However, a measurement that requires detailed observation is hard to achieve, especially on the infilling, aperture and weathering, and minimum physical observation is needed to overcome this limitation at the outcrop.
2. A higher resolution contributes to a higher amount of point cloud data. However, high resolution will limit the analysis ability of the computers and cause a longer time to process the data. On the other hand, filtering the point cloud data might reduce the resolution intensity. Thus, it is desirable to develop an appropriate generalisation algorithm that can reduce the density of insignificant points and, at the same time, maintain accuracy (Zam et al., 2018).
3. Some conditions are mutually exclusive. For example, if infilling is present, the roughness of the surface will be overshadowed by the influence of the gouge (Brook, 2016). Therefore a minimum close observation is required to overcome the limitation

Recommendations:

1. It is recommended that both types of acquisition methods are integrated (UAV and TLS) to analyse the rock slope stability. Due to the hazardous nature of the slope, only the slope surface could be scanned using TLS, and the top surface was difficult

to scan as well (case study 1). The UAV method enables the data collection to be carried out from the top surface. The TLS data can be integrated with the UAV to ensure that every part of the slope surface is scanned.

2. As all slopes are overhang the motorway, their vulnerability is always high. The narrow space between the slope and the road corridor leaves no other option. The factor of safety (FOS) of the rock slope needs to be analysed after determining the SMR and Kinematic Analysis of the rock slope.
3. The application of multispectral and thermal cameras by using UAV might be beneficial for slope stability analysis.

5. Conclusion

This paper proposed a different method for producing a 3D model of a rock slope for slope stability analysis using two case studies. The TLS method was used in the first case study and the second case study used an integrated UAV and TLS method. The result from the TLS at Ulu Choh Quarry has a shadow effect in some parts of the model, and the produced model is smaller than the 3D model of the Jelapang Rock Slope using an integrated UAV and TLS method. A clearer model, created with a more negligible shadow effect for the larger and wider Jelapang Rock Slope than the Ulu Choh Quarry, shows better production of the 3D surface model by integrating UAV and TLS data.

UAVs can be a compliment or replacement for terrestrial data acquisition methods. Given the shape, complexity, and dimensions of the rock slope, a combination of terrestrial and UAV (vertical and oblique) images would guarantee the completeness of the surveying, where a single point of view from TLS produces a shadow zone. The steps start with data acquisition during fieldwork, which takes about 2-3 days to fly the drone, set up the Terrestrial Laser

Scanner, and create the 3D point cloud. Then the site study is carried out through digital photogrammetry. Several software packages play an essential role in this process: Topcon Scan Master software, Topcon Magnetic Tools software, and Dips software. If the SMR index identifies areas with a high probability of failure, their GPS locations can be provided to the authorities to take further action.

The combination of a TLS and UAV survey, producing a 3D point cloud is seen as an alternative method to conventional geological surveying in rock slope stability analysis. The digital photogrammetric procedure speeds up the data acquisition phases and mitigates several drawbacks of the traditional mapping method. The software presented in this paper, Scan Master, is a recent approach to digital mapping on the 3D rock slope model. The geologist can define and measure all visible joints, even with extensive data, through this new technique. An advancement of this computational application allows distinguishing between natural and man-made joints to avoid the common mistakes in the traditional method. This technique provides comprehensive information on discontinuities and slope geometry that would most benefit rock slope analysis in remote, inaccessible, and broad areas. Other benefits of this approach are high geometric accuracy relating to the possibility of drones travelling near to the rock slope surface (up to a few metres away), deterrence of dangerous incidents during walkover surveys, and inexpensive data collection.

The 3D point cloud produced by the combination of TLS and UAV data is reliable in determining the possible occurrence of slope failure. Comparing the data with the direct classical method proved that both techniques are accurate in their measurements. According to the kinematic analysis, field and point cloud analyses resulted in an identical type and a very close probability of rock slope failure. However, the quality of the point cloud acquired through

UAV and TLS significantly depends on the camera used, the number and quality of the pictures, the data acquisition strategy, the selected ground control points, and the vertical and horizontal alignment of the raw 3D Point Cloud. Therefore, these results must be interpreted with caution.

Data from the combined TLS-UAV method can be represented in orthophotographs and 3D models integrated into a GIS. This product will be readily available and appropriate for classifying slopes in diversified hazard groups to create a valuable method for safe preparation and decision-making related to rock slopes.

Acknowledgements

All of the authors would like to thank PLUS Sdn Bhd and Universiti Teknologi Malaysia for providing the Contract Research DTD grants as listed below to carry out this study:

1. Rock Slope Monitoring And Surveillance Using Terrestrial Laser Scanning (TLS) And Global Positioning Systems (GPS) (R.J130000.7651.4C253).
2. Development of a comprehensive model for rock slope monitoring using infra-red thermal remote sensing on UAV platform (R.J130000.7652.4C255).
3. Evaluating and monitoring the effects of climate changes on landslide hazard zonation using Artifical Neural Network and real-time monitoring system (Q.J130000.2451.09G23).

References

Abellán, A., Oppikofer, T., Jaboyedoff, M., Rosser, N.J., Lim, M. and Lato, M.J. (2014). Terrestrial laser scanning of rock slope instabilities. Earth surface processes and landforms, 39(1), 80-97.

Agisoft, L.L.C., (2016). Agisoft PhotoScan User Manual. Professional Edition, Version 1.2, 37.

Akgul, M., Yurtseven, H., Akburak, S., Demir, M., Cigizoglu, K., Ozturk, T., & Eksi, M. (2016, June). Terrestrial laser scanning based pavement degradation monitoring in the winter season. In 1st International Symposium of Forest Engineering and Technologies (pp. 02-04).

Alam, M. M., & Sadique, M. R. (2021). Comparison of Slope Mass Ratings Classification Systems: A Review.

Azarafza, M., Asghari-Kaljahi, E., & Akgün, H. (2017). Assessment of discontinuous rock slope stability with block theory and numerical modeling: a case study for the South Pars Gas Complex, Assalouyeh, Iran. Environmental Earth Sciences, 76(11), 1-15.

Azarafza, M., Asghari-Kaljahi, E., & Akgün, H. (2017). Numerical modeling of discontinuous rock slopes utilising the 3DDGM (three-dimensional discontinuity geometrical modeling) method. Bulletin of Engineering Geology and the Environment, 76(3), 989-1007.

Azarafza, M., Koçkar, M. K., & Zhu, H. H. (2021). Correlations of SMR-Qslope Data in Stability Classification of Discontinuous Rock Slope: A Modified Relationship Considering the Iranian Data. Geotechnical and Geological Engineering, 1-14.

Bieniawski, Z.T. (1979) The geomechanics classification in rock engineering application. Proc. 4th Congress of the Internat. Soc. Rock Mechanics, v.2, 41–48.

Brook, M. S. (2016). Geomechanical behaviour and deformation of coal mine roof strata around faults: toward an engineering geological model. Master Master's Thesis, University of New South Wales

Buckley, S.J., Kurz, T.H., Howell, J.A. and Schneider, D., (2013). Terrestrial lidar and hyperspectral data fusion products for geological outcrop analysis. Computers & Geosciences, 54, 249-258.

Chanut, M. A., Gasc-Barbier, M., Dubois, L., & Carotte, A. (2021). Automatic identification of continuous or non-continuous evolution of landslides and quantification of deformations. Landslides, 1-18.

Chen, N., Cai, X., Li, S., Zhang, X., & Jiang, Q. (2021). Automatic extraction of rock mass discontinuity based on 3D laser scanning. Quarterly Journal of Engineering Geology and Hydrogeology, 54(1).

Compton, R. R., & Compton, R. R. (1985). Geology in the Field (p. 416). New York: Wiley.

Danzi, M., Di Crescenzo, G., Ramondini, M., & Santo, A. (2013). Use of unmanned aerial vehicles (UAVs) for photogrammetric surveys in rockfall instability studies. Rendiconti Online Societa Geologica Italiana, 24, 82-85.

Di Crescenzo G & Santo A. (2007) - High-resolution mapping of rockfall instability through the integration of photogrammetric, geomorphological and engineering– geological surveys. Quaternary International 171–172, 118– 130.

Feng, Q., (2012). Practical application of 3D laser scanning techniques to underground projects. ISRM-Swedish national task A survey of 3d laser scanning techniques for application to rock mechanic, BeFo Report, 114, 67.

Ferrero A.M., Migliazza M., Rocella R. & Segalini A. (2011) - Rock cliffs hazard analysis based on remote geostructural surveys: The Campione del Garda case study (Lake Garda, Northern Italy). Geomorphology 125, 457– 471.

Frayssines, M., & Hantz, D. (2006). Failure mechanisms and triggering factors in calcareous cliffs of the Subalpine Ranges (French Alps). Engineering Geology, 86(4), 256-270.

Frodella, W., Gigli, G., Morelli, S., Lombardi, L., & Casagli, N. (2017). Landslide mapping and characterisation through infrared thermography (IRT): suggestions for a methodological approach from some case studies. Remote Sensing, 9(12), 1281.

Fröhlich, C. and Mettenleiter, M., (2004). Terrestrial laser scanning—new perspectives in 3D surveying. International archives of photogrammetry, remote sensing and spatial information sciences, 36(Part 8), W2

Fussell,F and Angela, A (1982). Terrestrial photogrammetry in archaeology. World Archaeology, 14(2), 157–172.

García-Sellés, D., Falivene, O., Arbués, P., Gratacos, O., Tavani, S. and Muñoz, J.A., (2011). Supervised identification and reconstruction of near-planar geological surfaces from terrestrial laser scanning. Computers & Geosciences, 37(10), 1584-1594.

Geosains, J. M. D. (2012). Geological Map of Peninsular Malaysia: Modified based on the 8th edition, 1985. Director-General of Minerals and Geoscience Malaysia.

Gili, J. A., Corominas, J., & Rius, J. (2000). Using Global Positioning System techniques in landslide monitoring. Engineering geology, 55(3), 167-192.

Grönwall, C., Rydell, J., Tulldahl, M., Zhang, E., Bissmarck, F., & Bilock, E. (2017). Two imaging systems for positioning and navigation. 2017 Workshop on Research, Education, and Development of Unmanned Aerial Systems (RED-UAS) 120-125. IEE E.

Guyer, J. P. (Ed.). (2017). An Introduction to Measurement of Rock Discontinuities and Quality Designation.

Guzzetti, F., Mondini, A. C., Cardinali, M., Fiorucci, F., Santangelo, M., & Chang, K. T. (2012). Landslide inventory maps: New tools for an old problem. Earth-Science Reviews, 112(1-2), 42-66.

Hantz, D., & Frayssines, M. (2009). Rock wall retreat and historical back analysis of failures in Alpine limestone cliffs. Landslide processes: from geomorphologic mapping to dynamic modelling, Strasbourg.

Hencher, S.R., (1987). The implications of joints and structures for slope stability. Slope Stability. John Wiley,145-186.

Hoek, E. and Bray, J. W., (1981), Rock Slope Engineering: The Institute of Mining and Metallurgy, London, England, 358

Ismail, A., Rashid, A. S. A., & Sa'ari, R. (2020, September). Application of Photogrammetric Technique in Determination of Rock Slope Stability of Quarry. In IOP Conference Series: Materials Science and Engineering (Vol. 932, No. 1, p. 012054). IOP Publishing.

ISRM (1981): Rock characterisation testing and monitoring. In: Brown, E. T. (ed.) Pergamon Press, Oxford.

ISRM Commission on Standardization of Laboratory and Field Tests (1978) 'Suggested Methods for the Quantitative Description of Discontinuities', International Journal of Rock Mechanics and Mining Sciences and Geomechanics. 15, 319-368.

Jaboyedoff, M., Oppikofer, T., Abellán, A., Derron, M.H., Loye, A., Metzger, R. and Pedrazzini, A., (2012). Use of LIDAR in landslide investigations: a review. Natural hazards, 61(1), 5-28.

Ji, J., & Liao, H. J. (2014). Sensitivity-base reliability analysis of earth slopes using finite element method. Geomechanics and Engineering, 6(6), 545-560.

Kumar, S., & Pandey, H. K. (2021). Slope Stability Analysis Based on Rock Mass Rating, Geological Strength Index and Kinematic Analysis in Vindhyan Rock Formation. Journal of the Geological Society of India, 97(2), 145-150

Kundu, J., Sarkar, K., Verma, A. K., & Singh, T. N. (2022). Novel methods for quantitative analysis of kinematic stability and slope mass rating in jointed rock slopes with the aid of a new computer application. Bulletin of Engineering Geology and the Environment, 81(1), 1-19.

Lato, M., Diederichs, M. S., Hutchinson, D. J., & Harrap, R. (2009). Optimisation of LiDAR scanning and processing for automated structural evaluation of discontinuities in rockmasses. International journal of rock mechanics and mining sciences (1997), 46(1), 194-199.

Lato, M. J., & Vöge, M. (2012). Automated mapping of rock discontinuities in 3D lidar and photogrammetry models. International journal of rock mechanics and mining sciences (1997), 54, 150-158.

Li, X., Liu, J., Gong, W., Xu, Y., & Bowa, V. M. (2022). A discrete fracture network based modeling scheme for analysing the stability of highly fractured rock slope. Computers and Geotechnics, 141, 104558.

Liu, B., He, K., Han, M., Hu, X., Wu, T., Wu, M., & Ma, G. (2021). Dynamic process simulation of the Xiaogangjian rockslide occurred in shattered mountain based on 3DEC and DFN. Computers and Geotechnics, 134, 104122

Long, Y., Huang, Q., Wu, F., Yi, H., Guan, S., & Sha, P. (2021, October). Automatic identification of irregular rock blocks from 3D point cloud data of rock surface. In IOP Conference Series: Earth and Environmental Science (Vol. 861, No. 2, p. 022048). IOP Publishing

Maazallahi, V., & Majdi, A. (2021). Directional rock mass rating (DRMR) for anisotropic rock mass characterisation. Bulletin of Engineering Geology and the Environment, 80(6), 4471-4499.

Matasci, B., Carrea, D., Abellan, A., Derron, M.H., Humair, F., Jaboyedoff, M. and Metzger, R., (2015). Geological mapping and fold modeling using Terrestrial Laser Scanning point clouds: application to the Dents-du-Midi limestone massif (Switzerland). European Journal of Remote Sensing, 48(1), 569-591.

Matsimbe, J. (2021). Comparative application of photogrammetry, handmapping and android smartphone for geotechnical mapping and slope stability analysis. Open Geosciences, 13(1), 148-165.

Mazzanti, P., Caporossi, P., Brunetti, A., Mohammadi, F. I., & Bozzano, F. (2021). Short-term geomorphological evolution of the Poggio Baldi landslide upper scarp via 3D change detection. Landslides, 1-15.

Morey, G. B. (1974). A modified dip-direction indicator. Journal of Sedimentary Research, 44(3).

Nex, F., & Remondino, F. (2014). UAV for 3D mapping applications: a review. Applied geomatics, 6(1), 1-15.

Oppikofer, T., Jaboyedoff, M., Blikra, L., Derron, M. H., & Metzger, R. (2009). Characterisation and monitoring of the Åknes rockslide using terrestrial laser scanning. Natural Hazards and Earth System Sciences, 9(3), 1003-1019.

Pantaweesak, P., Sontamino, P., & Tonnayopas, D. (2019). Alternative Software for Evaluating Preliminary Rock Stability of Tunnel using Rock Mass Rating (RMR) and Rock Mass Quality (Q) on Android Smartphone. Engineering Journal, 23(1), 95-108

Pastor, J. L., Riquelme, A. J., Tomás, R., & Cano, M. (2019). Clarification of the slope mass rating parameters assisted by SMRTool, an open-source software. Bulletin of Engineering Geology and the Environment, 78(8), 6131-6142.

Raja, S., (2013). Influence of structural discontinuities on slope stability (Doctoral dissertation, MSc Thesis, submitted to National Institute of Technology, Karnataka India).

Rasmussen, L. L. (2020). UnBlocksgen: A Python library for 3D rock mass generation and analysis. SoftwareX, 12, 100577.

Riquelme, A. J., Tomás, R., & Abellán, A. (2016). Characterisation of rock slopes through slope mass rating using 3D point clouds. International Journal of Rock Mechanics and Mining Sciences, 84, 165-176.

Romana, M. (1985) New Adjustment Ratings for Application of Bieniawski Classification to Slopes. Internat. Soc. Rock Mech., Salzburg, 49-53.

Schlatter, D.M., Larsen, U., Stensgaard, B.M. and Buller, G., 2010. Digital field data capture: The Geological Survey of Denmark and Greenland experiences in Greenland. EXPLORE, Newsletter of the Association of Applied Geochemists, 147, 2-14.

Smith, J. V., & Arnhardt, C. (2016). A New Assessment Method for Structural-Control Failure Mechanisms in Rock Slopes—Case Examples. AIMS Geosciences, 2(3), 214.

Stead, D., & Wolter, A. (2015). A critical review of rock slope failure mechanisms: the importance of structural geology. Journal of Structural Geology, 74, 1-23.

Sturzenegger, M., & Stead, D. (2009). Quantifying discontinuity orientation and persistence on high mountain rock slopes and large landslides using terrestrial remote sensing techniques. Natural Hazards and Earth System Sciences, 9(2), 267-287.

Oguchi, T., Yuichi, S. H., & Wasklewicz, T. (2011). Data sources. Developments in Earth Surface Processes, 15, 189-224.

Reshetyuk, Y. (2006). Investigation and calibration of pulsed time-of-flight terrestrial laser scanners (Doctoral dissertation, KTH).

Tan, W. H., Sun, Z. H., Li, N., & Jiang, X. H. (2015). Stochastic three-dimensional joint geometry model and the properties of REV for a jointed rock mass. In Advanced Materials Research (Vol. 1079, pp. 266-271). Trans Tech Publications Ltd

Tan, K., Zhang, W., Shen, F., & Cheng, X. (2018). Investigation of TLS intensity data and distance measurement errors from target specular reflections. Remote Sensing, 10(7), 1077.

Tomas, R., Cuenca, A., Cano, M., & García-Barba, J. (2012). A graphical approach for slope mass rating (SMR). Engineering Geology, 124, 67-76.

Tsai, Z. X., You, G. J. Y., Lee, H. Y., & Chiu, Y. J. (2012). Use of a total station to monitor post-failure sediment yields in landslide sites of the Shihmen reservoir watershed, Taiwan. Geomorphology, 139, 438-451.

Van Westen, C. J., Castellanos, E., & Kuriakose, S. L. (2008). Spatial data for landslide susceptibility, hazard, and vulnerability assessment: An overview. Engineering geology, 102(3-4), 112-131.

Walsh, S. J., Page, P. H., Brewington, L., Bradley, J. R., & Mena, C. F. (2018). A beach vulnerability framework for the Galapagos Islands: Fusion of worldview 2 imagery, 3-D laser scanner data, and unmanned aerial vehicles. Compr Remote Sens, 9, 159-176. 5

Wyllie, D.C., (2017). Stabilisation of rock slopes. In Rock Slope Engineering, 391-442.

Xu, Guochang X. Y., (2018). GPS: *Theory,* Algorithms and Applications. SPRINGER

Yakar, M., Yıldız, F., & Yılmaz, H. M. (2005). Tarihi Ve Kültürel Miraslarin Belgelenmesinde Jeodezi Fotogrametri Mühendislerinin Rolü. TMMOB Harita ve Kadastro Mühendisleri Odası, 10.

Yellas, C., Benzaid, R., & Tekkouk, M. (2021). Application of classification systems for the assessment of rock mass stability—case of national road 43, Jijel, Algeria. Arabian Journal of Geosciences, 14(3), 1-10.

Zam, P. M., Fuad, N. A., Yusoff, A. R., & Majid, Z. (2018). Evaluating the performance of terrestrial laser scanning for landslide monitoring. The International Archives of Photogrammetry, Remote Sensing and Spatial Information Sciences, 42, 35-55.

Zhuge, X. (2010). Short-range ultra-wideband imaging with multiple-input multiple-output arrays.

Zhou, J. W., Li, H. B., Zhou, Y., Zhang, J. Y., & Fan, G. (2021). Initiation mechanism and quantitative mass movement analysis of the 2019 Shuicheng catastrophic landslide. Quarterly Journal of Engineering Geology and Hydrology, 80

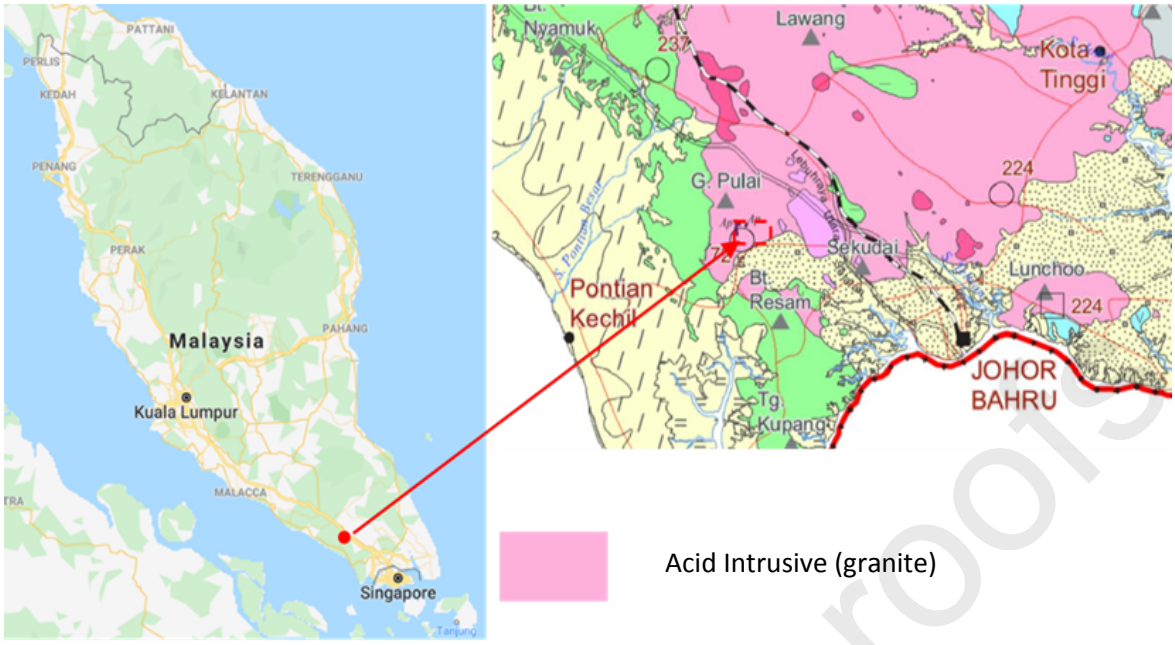

Figure 1: Location and General Geology of Case Study 1, Ulu Choh Quarry (Geosains, 2012).

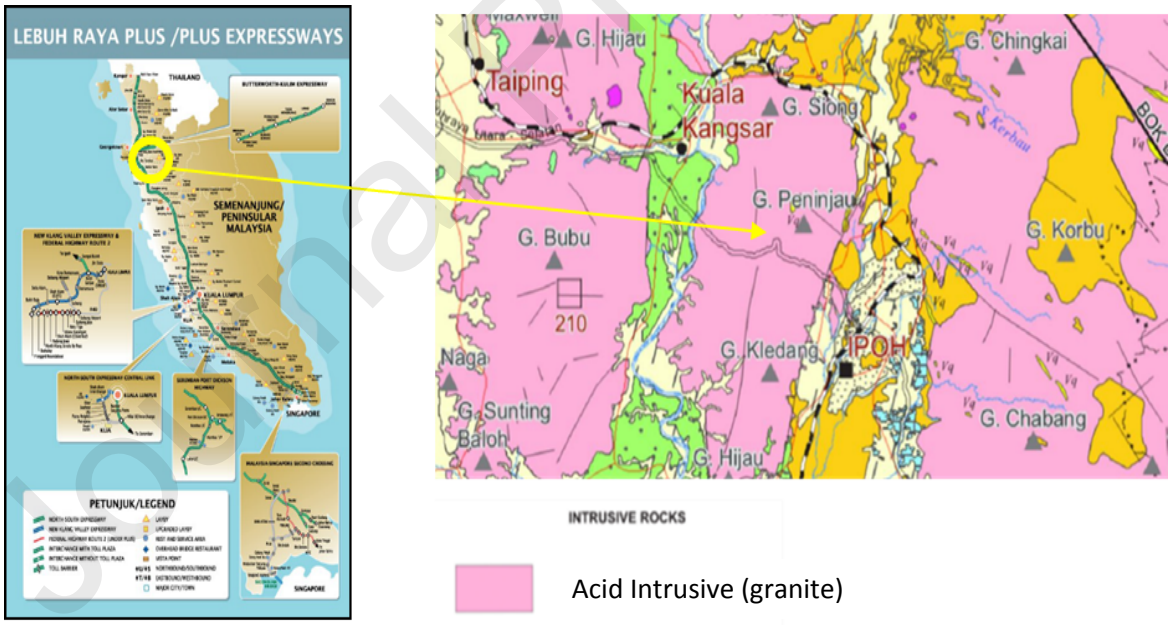

Figure 2: Location and General Geology of Case Study 2, Jelapang Rock Slope (Geosains,2012).

Figure 3: Rock Slope Structure at Jelapang.

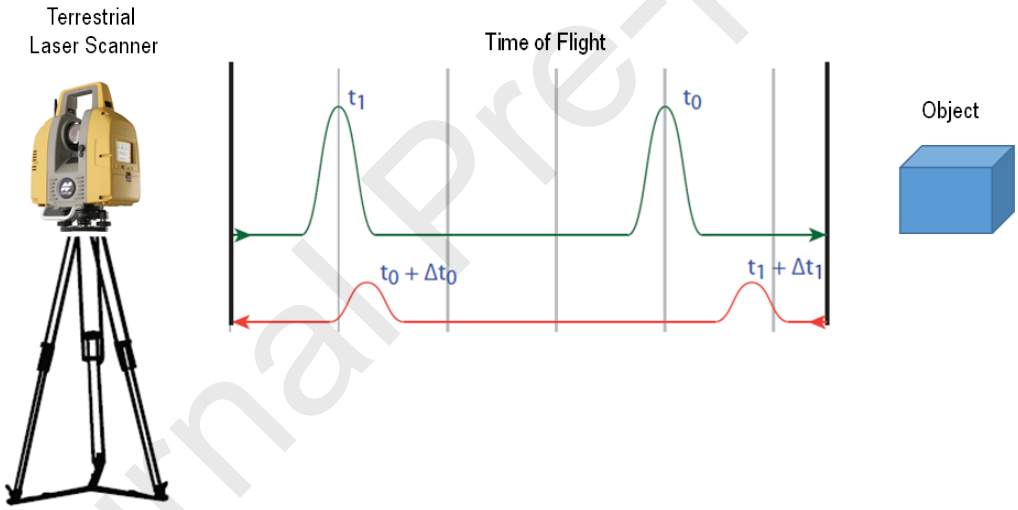

Figure 4: Distance measurement principle of time-of-flight laser scanners.

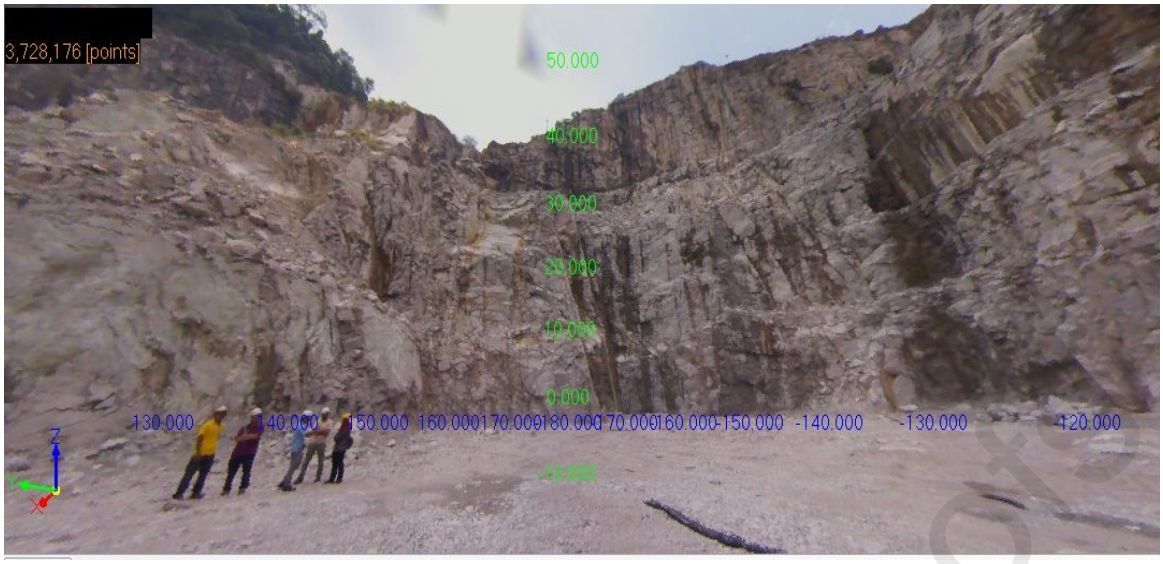

Figure 5: TLS internal camera at case study 1.

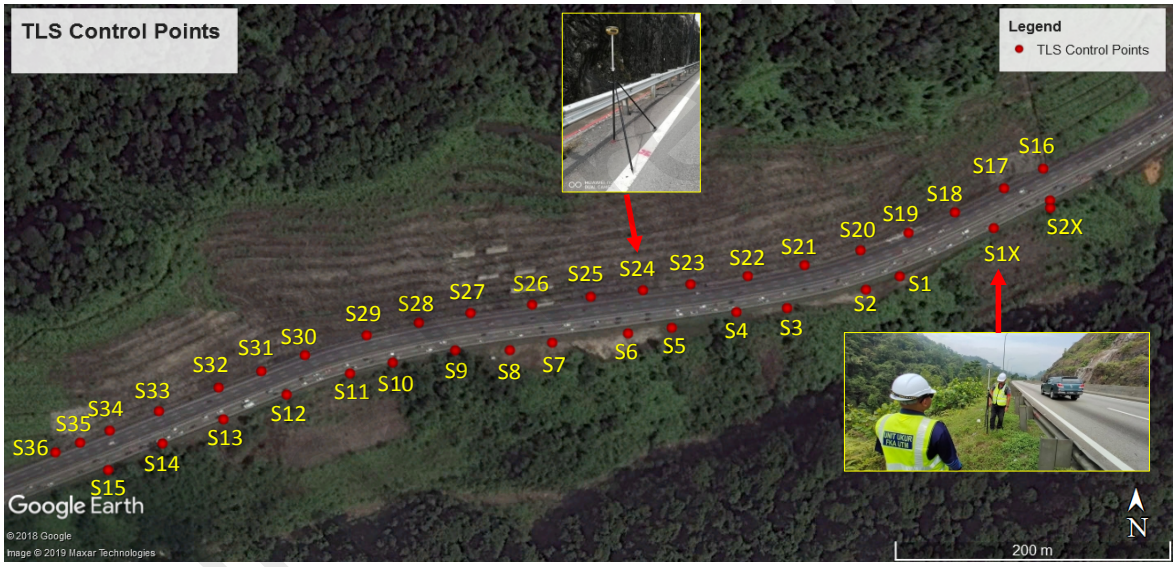

Figure 6: TLS measurement from reachable points along the rock slope (case study 2).

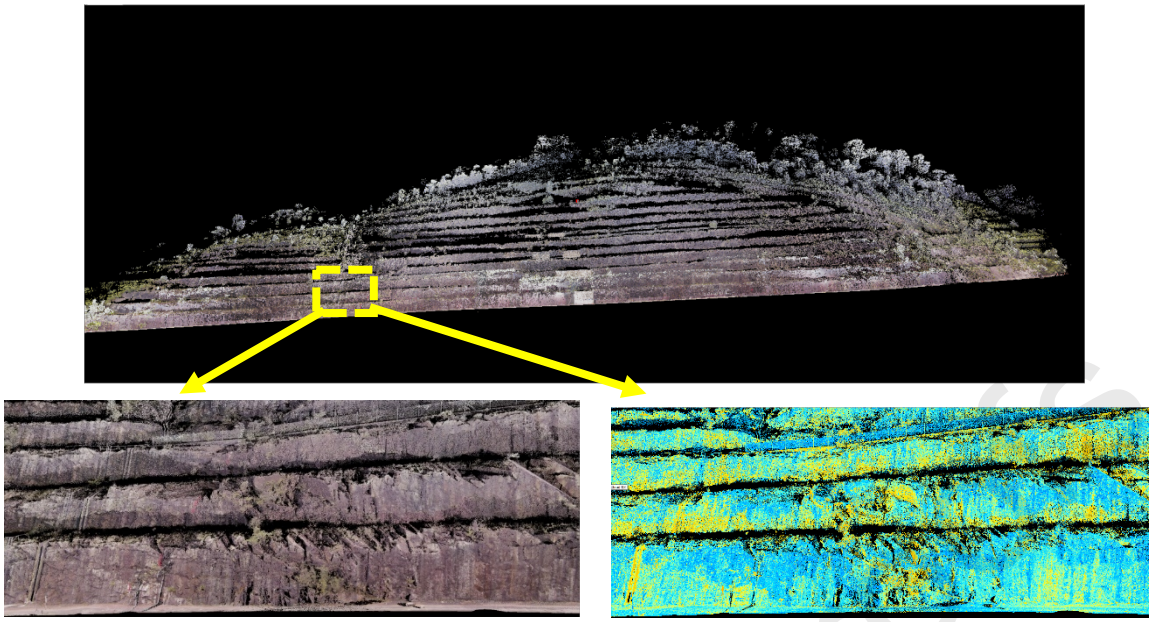

Figure 7: Solid model obtained by laser scanning of the slope (case study 2).

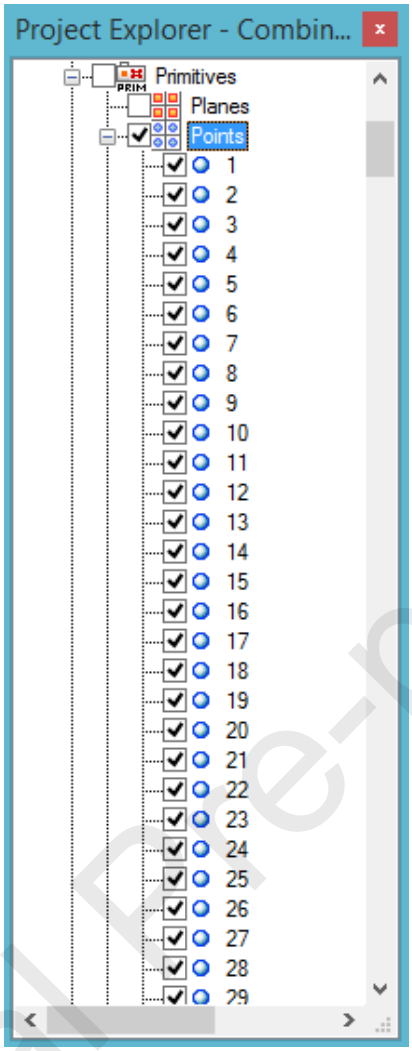

Figure 8: All the new points that were created appear in the point folder.

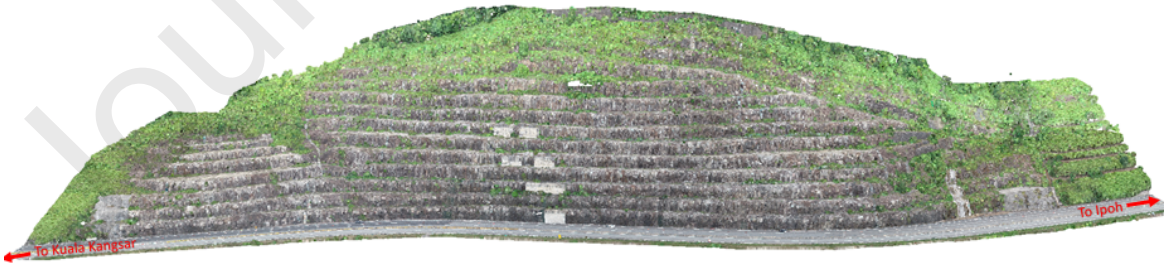

Figure 9: Hybrid point cloud from UAV and TLS (case study 2).

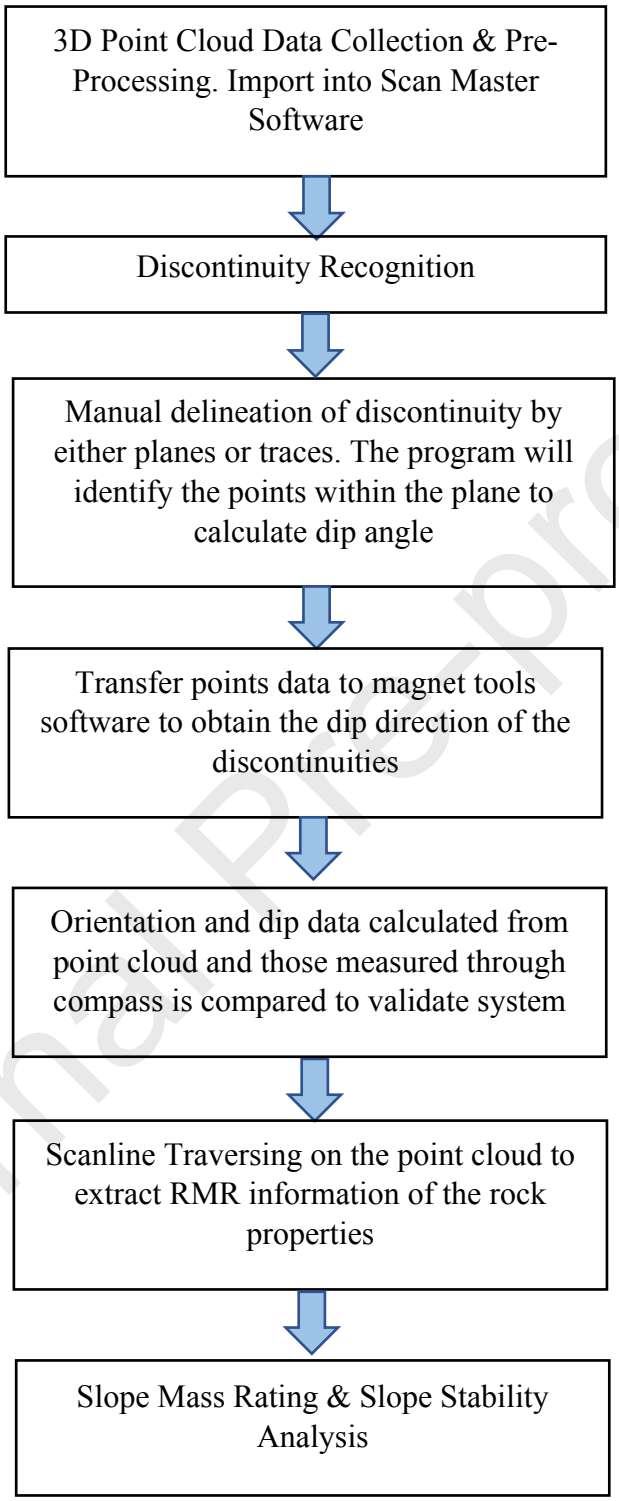

Figure 10: Methodological flow chart.

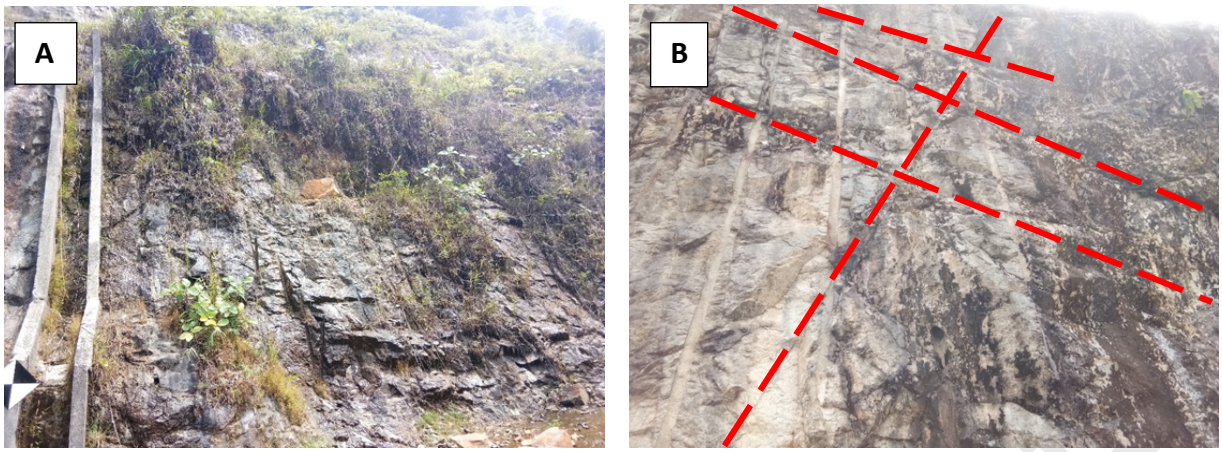

Figure 11: Insitu observation of A) water presence B) intersection of joints (case study 2).

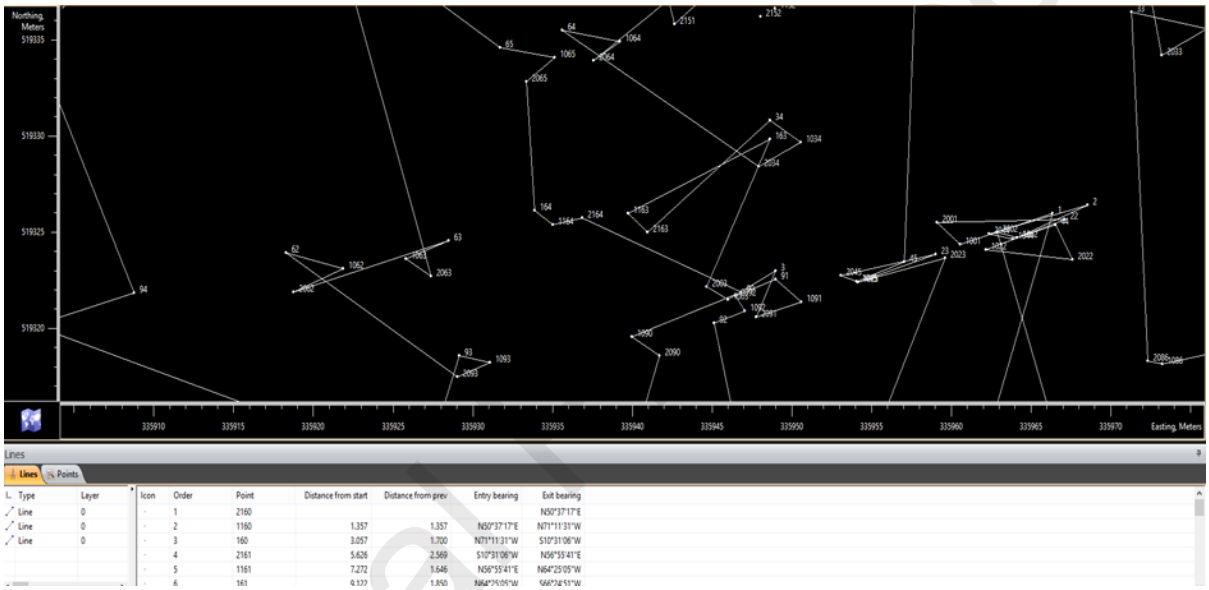

Figure 12: Data transferred to magnet tools software to measure Dip Direction of joint.

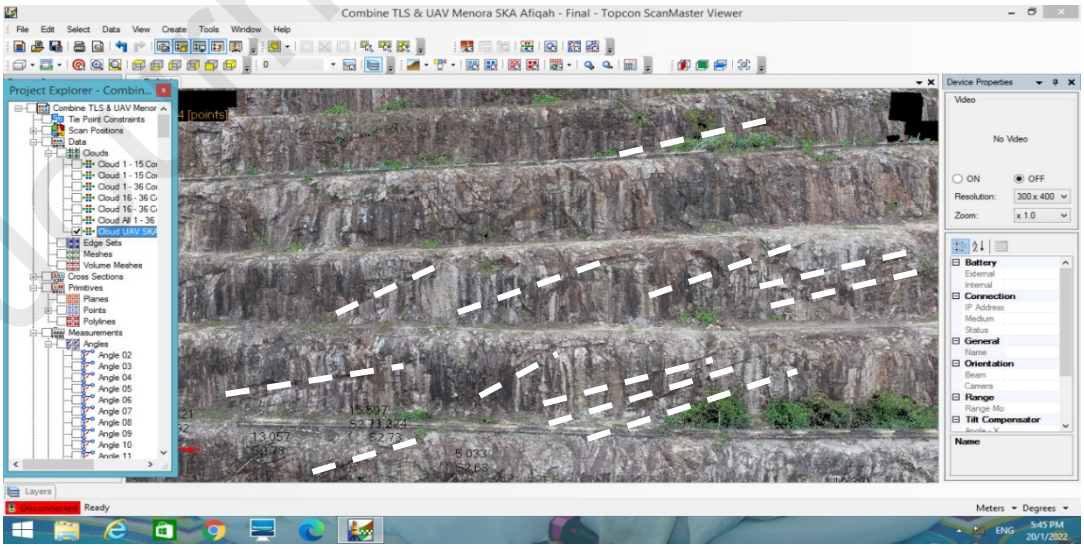

Figure 13: Principal Joint Set observed on the rock slope

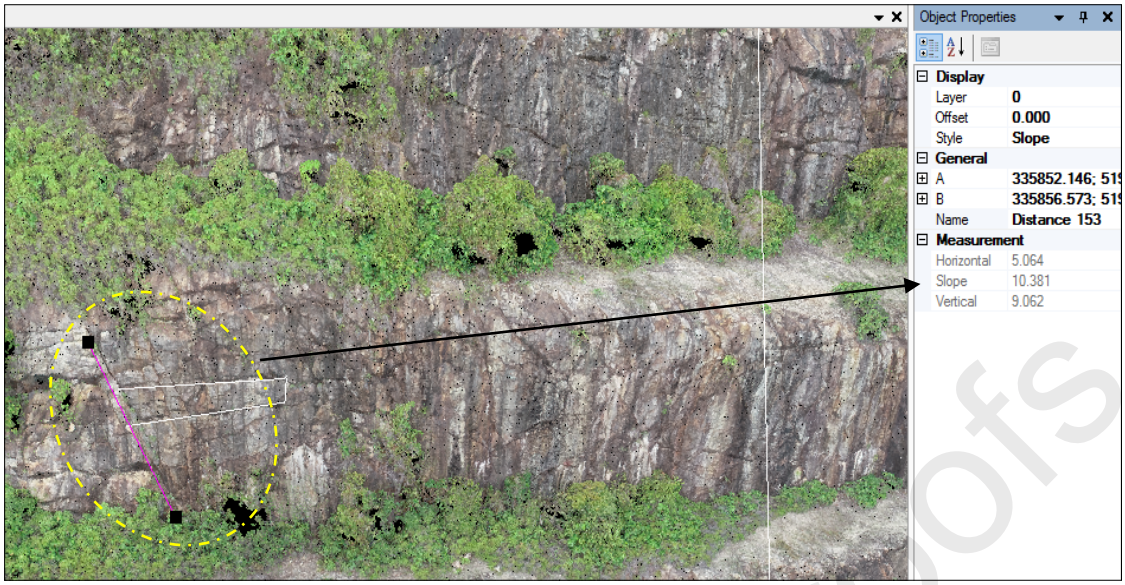

Figure 14: Persistence of the joint (purple line) measured is 10.3m.

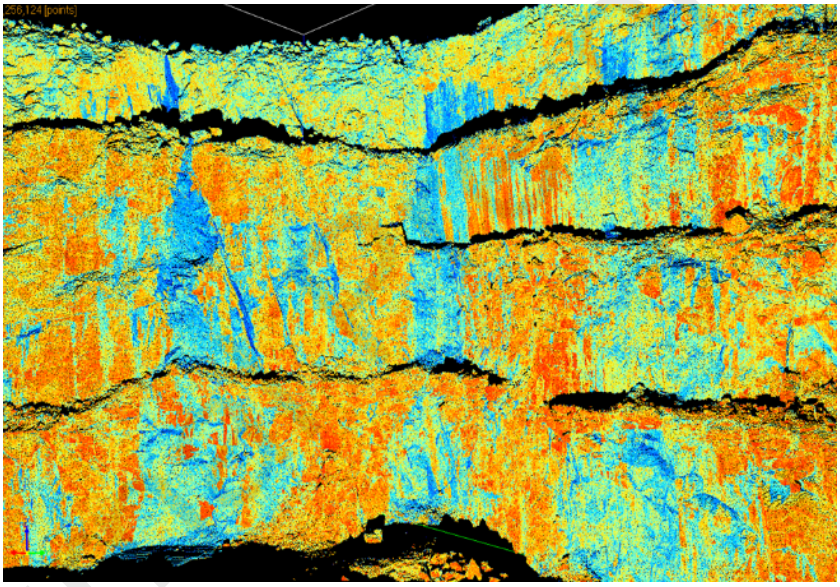

Figure 15: TLS image of Ulu Choh Quarry.

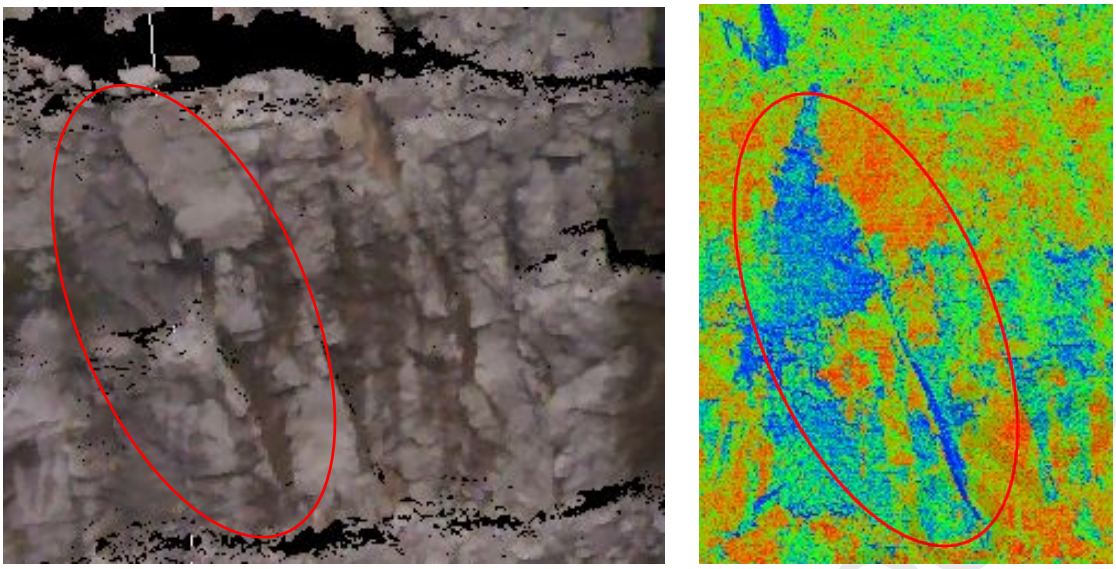

Figure 16: Joint found on rock slope through the TLS **.**

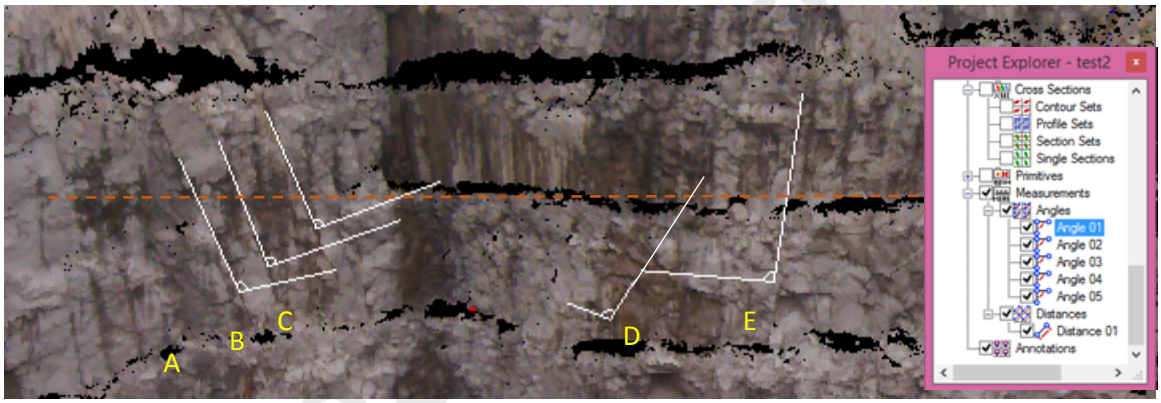

Figure 17: Joint A-E marked on the scanline

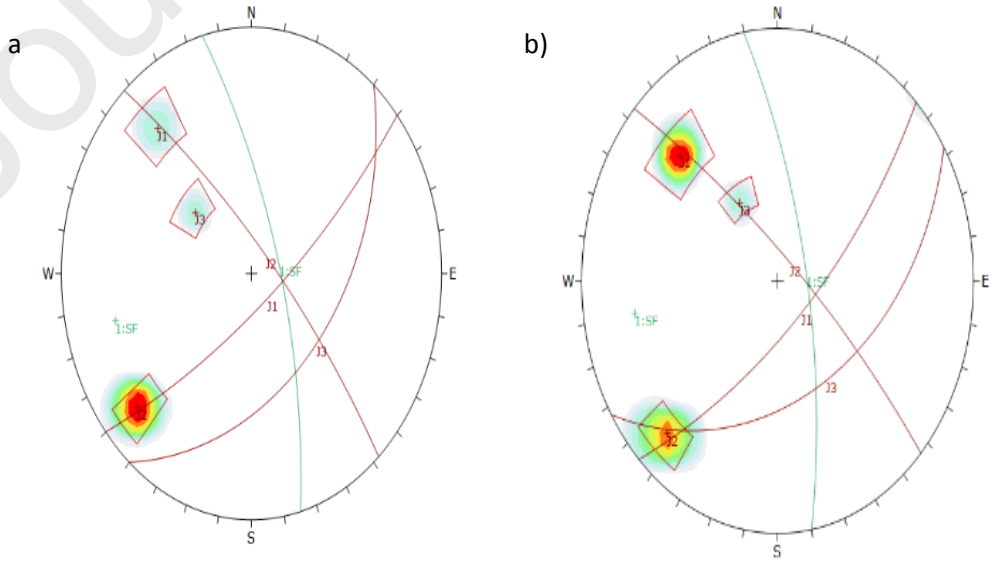

Figure 18: Contour plot of discontinuity plane for a) Terrestrial Laser Scanner b) Brunton Compass.

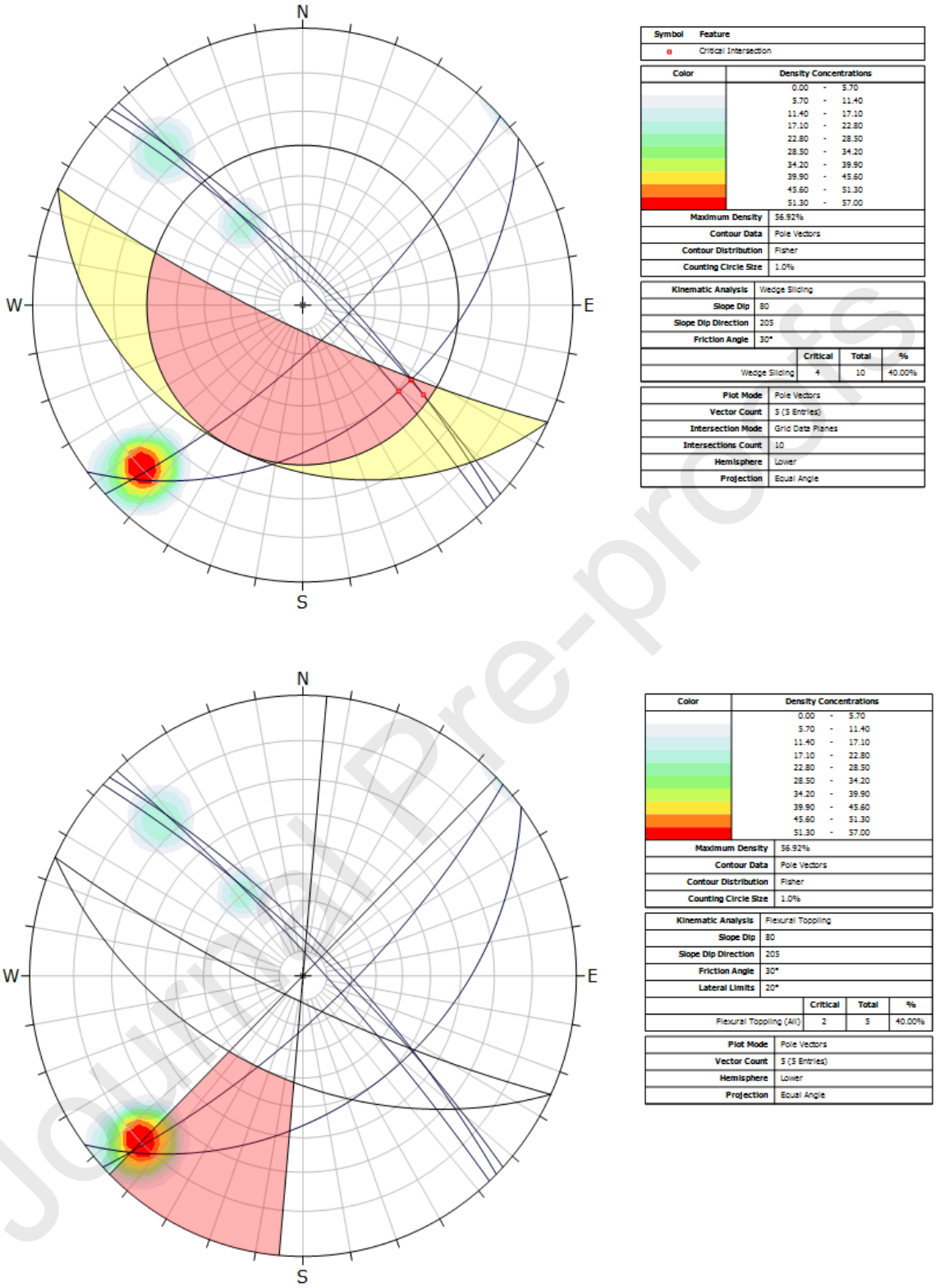

Figure 19: Flexural toppling and wedge failure are prominent type of failures that can occur at Ulu Choh Quarry.

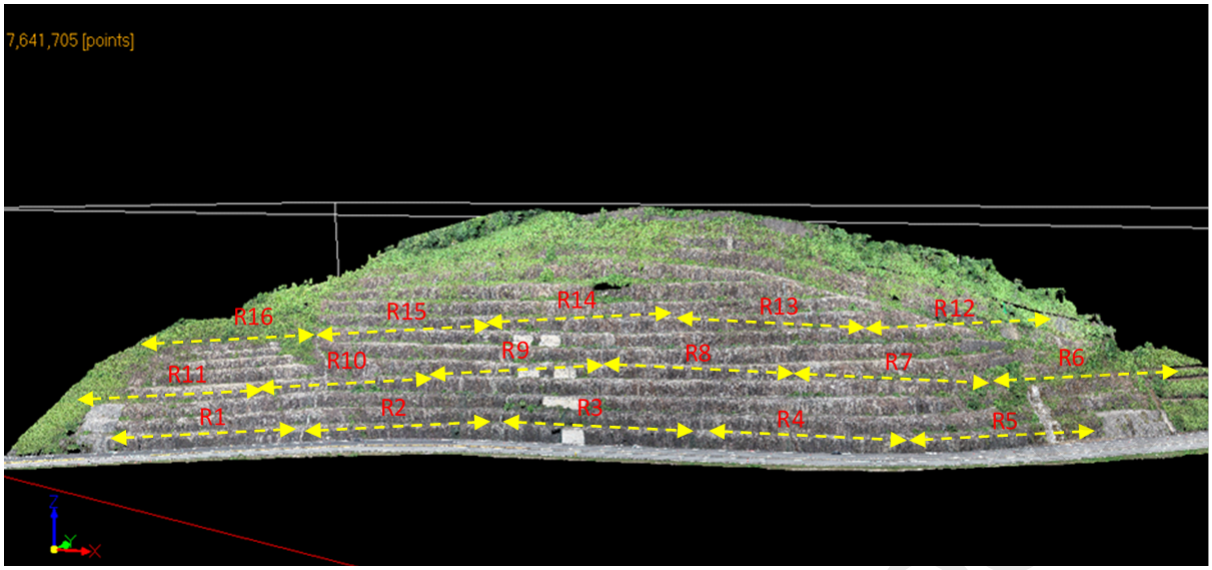

Figure 20: Jelapang Rock Slope is divided into 16 regions R1-R16.

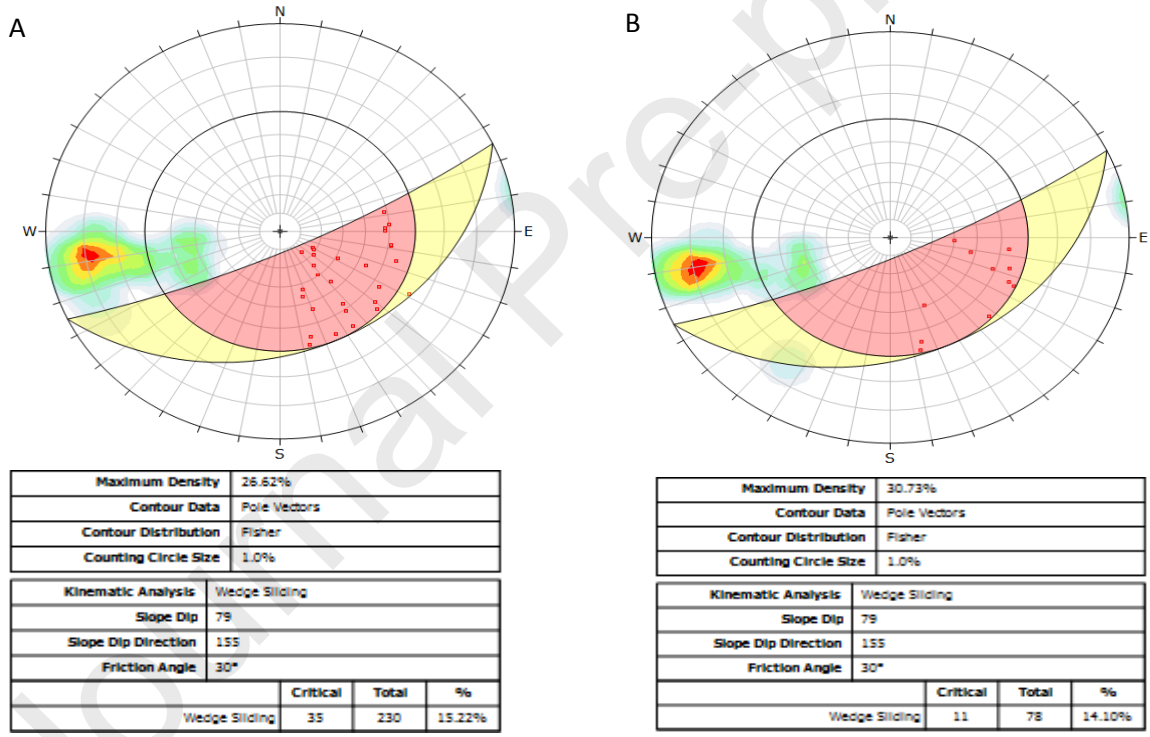

Figure 21: Stereographic projection of (A) Hybrid point cloud of TLS-UAV and (B) Brunton Compass survey.

Table 1: Overview of the advantages and disadvantages of different measurement techniques

Technique	Advantages	Disadvantages
Direct survey using Brunton Compass (Barnes,1981)	The Brunton compass has the advantages of combining a precise sighting-clinometer and hand level with a compass that can be used to measure bearings at either waist-height or eye height (Compton, 1985).	Difficulty in accessibility to the site, the limitations in using traditional tools to evaluate characteristics of large areas, and the restrictions in the identification and localisation of site features (Matasci et al., 2015) & Frayssines and Hantz (2006).
Global Positioning System (GPS) monitoring (Gili et al., 2000)	Provides information based on location in real time. Easy to be used by anyone	The accuracy of GPS depends on sufficient signal quality received. The GPS signal is affected by the atmosphere (i.e.multipath), Electromagnetic interference, ionosphere etc. This results in an error in the GPS signal of about 5 to 10 meters (Xu & Guochang, 2018).
Total Station measurement (Tsai et al., 2012, Palazo et al., 2006)	The accuracy of the total station is very high, but the low measurement speed limits overall efficiency and the number of cross-section points that can be measured (Wang et al., 2019).	Total station measurement accuracy has environmental problems such as light which cannot give the best results. Pricey and required skill personnel (Wang et a., 2019).
Close range photogrammetry (Wang et al., 2019)	Unaccessible parts (high, very low, dangerous) can be measured. Outcomes are detailed (Mustafa et al., 2009)	The lack of adequate lighting reduces the quality of the photographs (Yakar, Yildiz, and Yilmaz, 2005).
Ground Measuring Robot	Ability to produce spatially resolved measurements that are also reactive to on-the-ground conditions (Qian et al., 2017).	Limited spatial coverage. (Qian et al., 2017).
Synthetic aperture radar interferometry (Wang et al., 2018)	Simpler design process Flexible to change the scanning scheme Simpler processing scheme for focusing (Zhuge & Xiaodong, 2010).	In a region with rugged terrain and dense vegetation coverage, there are very limited to monitor different geohazards at a large scale (Zhang 2016 et al.). Limited data acquisition speed, require a larger number of scan position or antenna pairs, Collect only part of scattering matrix (Zhuge & Xiaodong, 2010)

Terrestrial Optical Photogrammetry (TOP)	High speed of on-site recording and the vast amount of detail that can be retrieved from the images (Fussell & Angela, 1982).	Not operating during the night, Very sensitive to change in acquisition geometry and surface state variations, expensive instrumentation and the delay in obtaining the results after the photography has been completed (Fussell & Angela, 1982).
Terrestrial Laser Scanner (TLS)	high precision and spatial resolution (Buckley, 2012) ability to specify and detect rock types from a distance accurately, accumulate a large number of measurements in inaccessible vertical areas, and perform fast and accurate data collection over wide areas (Abellán et al., 2014).	Require large memory space that cannot be handled by computer (Zam et al., 2018)
Unmanned Aerial Vehicle (Jaboyedoff et al., 2012)	The advantages of implementing and using UAVs in general include (Karas et al., 2016): - high-quality images obtained by aerial mapping of the area, - simple implementation, - management and decision support, - safe use subject to a UAV license.	The basic limitations are (Karas et al., 2016): - privacy, - technical failures of the navigation system, - distrust of new technologies, - legislation.

Table 2: Surveying instrument with a specification for TLS.

Instrument	Specification
Topcon TLS 2000 	Time of flight (TOF) Measurement Distance accuracy: 3.5mm@10m Laser Wavelength: 1064nm Scan rate: 120,000 points/sec Maximum scanning distance: 350m Internal Camera: 5mp Integrated
RTK GPS Ground Control Point (Topcon Hyper II and-SOUTH Galaxy G1)) 	Channels: 72 to 222 Channels Support GPS, Glonass and BDS Satellites Base and Rover for Precise RTK Survey Accuracy : 1cm (Horizontal) Accuracy : 2cm (Vertical)

Table 3: Software and its specifications.

Software	Specifications
Scan Master Software 	Point Clouds Data Processing: Data Editing Data Resampling Data Filtering Data Colourizing Import/Export
Topcon Magnet Officer Tool 	Static Post Processing RTK Post Processing Coordinate Transformation

Table 4: Surveying instrument with a specification for UAV.

Instrument	Specification
DJI Phantom 4 	Payload: 1.38 kg Flight Autonomous: 28 minutes Velocity Range: 2 m above ground Altitude Range: 0 - 10 m Operating Range: 0 - 10 m Obstacle Sensory Range: 0.7 - 15 m
MAPIR Survey2 (NIR and RGB sensors) 	Focal length: 35 mm Sensor: 20 megapixels Spatial resolution: 0.0134 x 0.0134 mm FOV: 60□ (horizontal) Capture Speed: RAW+JPG: 3 Seconds / Photo. JPG: 2 Seconds / Photo

Table 5: RMR parameters, method of acquisition, and data source.

Parameter	Acquisition	Data source
X1: Strength of rock material	Schmidt Hammer, UCS	Field, laboratory
X2: RQD	Geometric Analysis	Field, 3D photogrammetry
X3: Spacing of Discontinuity	Geometric Analysis	Field, 3D photogrammetry
X4: Condition of Discontinuity		
- Discontinuity Length	Geometric Analysis	Field, 3D photogrammetry
- Aperture	Geometric Analysis	Field, 3D photogrammetry
- Roughness	Geometric Analysis	Field, 3D photogrammetry
- Infilling	Geometric Analysis	Field, 3D photogrammetry
- Weathering	Visual Inspection	Field, images
- Groundwater	Water Index, Visual Observation	Field, NDWI

Table 6: Adjustment factor of SMR.

	Type of failure		Auxiliary angles	Very favorable	Favorable	Normal	Unfavorable	Very unfavorable
Parallelism	P	A=	$\lvert\alpha_j - \alpha_s\rvert$	> 30°	30 – 20°	20 – 10°	10 – 5°	< 5°
	T		$\lvert\alpha_j - \alpha_s - 180\rvert$					
	W		$\lvert\alpha_i - \alpha_s\rvert$					
	P/T/W	F_1		0.15	0.40	0.70	0.85	1.00
Dip angle	P/W	B=	β_j or β_i	< 20°	20 – 30°	30 – 35°	35 – 45°	> 45°
	P/W	F_2		0.15	0.40	0.70	0.85	1.00
	T					1.00		
Dip relationship	P	C=	$\beta_j - \beta_s$	> 10°	10 – 0°	0°	0 – (–10)°	< (–10)°
	W		$\beta_i - \beta_s$					
	T		$\beta_j + \beta_s$	< 110°	110 – 120°	> 120°	-	-
	P/T/W	F_3		0	-6	-25	-50	-60

Excavation method (F_4)			
Natural slope	+15	Blasting or mechanical	0
Presplitting	+10	Deficient blasting	-8
Smooth blasting	+8		

Table 7: Dip and strike from TLS and hand measurement by using Brunton compass.

	Terrestrial Laser Scanner (TLS)		**Compass (hand measurement)**	
	Dip	Dip Direction	Dip	Dip Direction
A	83	47NE	80	50NE
B	79	43NE	78	45NE
C	76	50NE	75	45NE
D	44	143SE	40	145SE
E	74	137SE	75	140SE

Table 8: Rock Mass Rating for Ulu Choh Quarry.

Rock Parameters		RMR
UCS Rating		4
RQD Rating		20
Spacing		8
Discontinuity Rating (R3)	Persistence	2
	Aperture	4
	Roughness	3
	Infilling	6
	Weathering	5
	Total	20
Groundwater Rating		15
Rock Mass Rating (RMR)		67
Rock Mass Class		II
Rock Mass Description		GOOD

Table 9: SMR analysis for Ulu Choh Quarry.

Slope Orientation	**Joints Orientation**			**Observed failure**	F1	F2	F3	F4	**f1xf2xf3**	**RMR Basic**	**SMR**	**Description**	**Stability**
	J1	J2	J3										
205/78	045/80	143/40	137/74	Wedge	0.15	0.85	-6	0	-0.765	67	66.235	Good	Stable

Table 10: Dip and Dip direction of the joint extracted from the TLS-UAV Point Cloud.

Chainage	Dip	Dip Direction
0.1	82	N78° 54’16’’E
0.5	66	75 SE
3	76	S79° 53’42’’E
6	65	S78° 18’43’’E
14	40	S83° 48’33’’E
18	70	S77° 44’10’’W
23	60	S79° 37’10’’W
25	85	S79° 37’10’’W
38	50	S87° 39’57’’E
40	80	65 SW
44	74	S87° 39’57’’E
49	74	S87° 39’57’’E
58	33	S77°09 ’52’’W
63	85	S80° 57’32’’E
66	80	S71°29 ’50’’W
73	46	S79°52 ’29’’W
78	42	S89°03 ’57’’E
80	46	60 SW
92	45	S62°43 ’28’’W
100	80	S62°43 ’28’’W

Table 11: Dip and Dip Direction of the joint obtain by using Brunton Compass survey.

Chainage	Dip	Dip Direction
0	80	79 SW
3.2	75	75 SE
8.2	70	76 SE
14	38	80 SE
17.8	61	76SW

19	58	65 SW
21	43	60 SE
24.8	85	79 SW
49	74	87 SE
62	85	80 SE
64	73	35 SW
78	45	80 SW
90	45	61 SW

Table 12: Slope and Joint Orientation.

Rock Slope No		**Joints Orientation**			**Observed failure based on the stereonet**
R1	**Slope Orientation**	J1	J2	J3	
R1	115/75	80/120	37/236	46/95	Planar/Wedge
R2	130/80	75/258	88/116	75/88	Planar/Wedge
R3	130/78	50/220	70/112		Small blocks
R4	130/75	52/258	65/85	46/74	Wedge
R5	135/78	60/265	56/95	40/70	Planar/Wedge/Topple
R6	140/79	88/116	66/242	75/088	Planar/wedge
R7	140/75	70/112	45/220	74/078	wedge
R8	140/82	70/103	52/257	46/074	Planar/ Wedge/ Topple
R9	150/75	56/106	50/249	65/085	wedge
R10	140/73	80/105	67/234	55/306	planar/wedge
R11	140/72	86/156	65/113	67/085	planar/wedge
R12	010/72	56/106	50/249	65/085	wedge
R13	010/73	80/105	67/234	55/306	wedge
R14	150/76	86/156	65/113		wedge
R15	120/78	50/111	32/259		planar/wedge
R16	100/80	75/110	35/248	46/75	planar/wedge

Table 13: Rock Mass Rating (RMR) for every region.

Rock Slope No		**R1**	**R2**	**R3**	**R4**	**R5**	**R6**	**R7**	**R8**	**R9**	**R10**	**R11**	**R12**	**R13**	**R14**	**R15**	**R16**
UCS		12	7	7	4	4	4	4	4	7	4	4	4	4	4	4	4
RQD		20	20	20	20	20	20	20	20	20	20	20	20	20	20	17	20
Spacing		15	20	20	15	20	10	15	20	20	15	15	8	15	15	15	20
discontinuity Rating (R3)	P*	1	1	2	2	1	1	1	1	2	2	2	2	2	1	1	1
	A*	4	1	5	1	1	1	4	1	5	5	1	1	4	1	1	4
	R*	5	3	3	3	3	3	3	3	5	3	1	3	1	3	3	3
	I*	4	4	4	2	4	4	4	2	4	2	2	2	2	2	2	4
	W*	5	5	5	5	5	3	5	5	5	5	5	1	3	3	3	5
Total		19	14	19	13	14	13	19	12	19	17	11	9	12	9	10	17
Ground		10	10	10	10	10	15	15	10	15	15	15	10	15	15	15	15
Rock Mass Rating (RMR)		76	71	76	62	68	61	73	66	83	71	64	51	66	64	61	76
Rock Mass Class		II	II	II	II	II	II	II	II	II	II	II	II	II	II	II	II
Rock Mass Description		G	G	G	G	G	G	G	G	VG	G	G	F	G	G	G	G

Table 14: Slope Mass Rating.

Rock Slope No	RMR Basic	Observed failure	The factorial adjustment factor				SMR Rating	Class no	Slope Description	Stability	Inferred failure from SMR	Chances for specific failure mode to fail
			F1	F2	F3	F4						
1	76	Planar/Wedge	1	0.15	-50	8	76.5	II	Good	Stable	Some block failure	20%
2	71	Planar/Wedge	0.15	0.4	-25	8	77.5	II	Good	Stable	Some block failure	20%
3	76	Small blocks	0.4	0.4	-25	8	80	II	Good	Stable	Some block failure	20%
4	62	Wedge	0.4	0.15	-25	8	68.5	II	Good	Stable	Some block failure	20%
5	68	Planar/Wedge/Topple	0.15	1	-6	8	75.1	II	Good	Stable	Some block failure	20%
6	61	Planar/wedge	0.4	1	-25	8	59	III	Fair	Partially Stable	Planar along joints or wedge failure	40%
7	73	wedge	0.4	0.15	-25	8	79.5	II	Good	Stable	Some block failure	20%
8	66	Planar/ Wedge/ Topple	0.4	0.4	-25	8	70	II	Good	Stable	Some block failure	20%
9	83	wedge	0.4	0.15	-50	8	88	I	Very Good	Stable	No failure	0%

10	71	planar/wedge	0.4	0.4	-50	8	71	II	Good	Stable	Some block failure	20%
11	64	wedge	0.4	0.4	-50	8	64	II	Good	Stable	Some block failure	20%
12	51	wedge	0.4	1	-50	8	39	IV	Bad	Unstable	Planar or Big Wedge	60%
13	66	wedge	0.4	0.4	-60	8	50	III	Fair	Partially Stable	Planar along joints or wedge failure	40%
14	65	planar/wedge	0.4	1	-50	8	53	III	Fair	Partially Stable	Planar along joint or wedge failure	40%
15	61	planar/wedge	0.15	0.4	-50	8	66	II	Good	Stable	Some block failure	20%
16	76	planar/wedge	0.4	0.15	-50	8	81	II	Good	Stable	Some block failure	20%

	Type of failure		Auxially Angles	Very Favourable	Favourable	Normal	Unfavourable	Very unfavourable
Parallelism	P		$\lvert \alpha_j-\alpha_s \rvert$					
	T	A=	$\lvert \alpha_j-\alpha_s-180 \rvert$	>30º	30-20º	20-10º	10-5º	<5º
	W		$\lvert \alpha_j-\alpha_s \rvert$					
	P/T/W	F_1		0.15	0.40	0.70	0.85	1.00
Dip Angle	P/W	B=	β_j	<20º	20-30º	30-35º	35-45º	>45º
	P/W	F_2		0.15	0.40	0.70	0.85	1.00
	T					1.00		
Dip Relationship	P		$\beta_j-\beta_s$					
	W	C=	$\beta_j-\beta_s$	>10º	10-0º	0º	0-(-10º)	<(-10º)
	T		$\beta_{j+}\beta_s$	<110º	110-120º	>120º	-	-
	P/W/T	F_3		0	-6	-25	-50	-60

Excavation Method (F_4)			
Natural Slope	+15	Blasting or Mechanical	0
Presplitting	+10	Deficient Blasting	-8
Smooth Blasting	+8		

Table 6: Adjustment factor of SMR.

FAILURE: P planar; T toppling. DIP DIRECTION: α_j discontinuity; α_s slope. DIP: β_j discontinuity ; β_s: slope .

The highlight of the paper

1. The conventional geological mapping in determining rock slope stability is risky and costly.
2. The laser scanning and drone photogrammetric techniques allow it to overcome these issues by remotely collecting highly detailed point cloud data of a rock slope.
3. This research compares the integration of Unmanned Aerial Vehicle (UAV) and TLS photogrammetry with traditional direct methods.
4. The results show that both techniques provide accurate measurement and analysis compared to the traditional direct method.

CREDIT AUTHOR STATEMENT

APPLICATION OF COMBINED TERRESTRIAL LASER SCANNING AND UNMANNED AERIAL VEHICLE DIGITAL PHOTOGRAMMETRY METHOD IN HIGH ROCK SLOPE STABILITY ANALYSIS: A CASE STUDY

Afiqah Ismail - Writing - Original Draft, Methodology, Software, Validation, Investigation

Ahmad Safuan A Rashid – Conceptualization, Supervision, Writing - Review & Editing, Project administration

Radzuan Sa'ari – Methodology, Software

Abd Wahid Rasib – Conceptualization, Software

Mushairry Mustaffar - Software

Rini Asnida Abdullah - Methodology

Azman Kassim - Methodology

Norbazlan Mohd Yusof - Funding acquisition, Project administration

Norisam Abd Rahaman - Funding acquisition, Project administration

Roohollah Kalatehjari - Writing - Review & Editing

Declaration of interests

☒ The authors declare that they have no known competing financial interests or personal relationships that could have appeared to influence the work reported in this paper.

☐The authors declare the following financial interests/personal relationships which may be considered as potential competing interests:

Authors

Afiqah Ismail

Ahmad Safuan A Rashid

Radzuan Sa'ari

Abd Wahid Rasib

Mushairry Mustaffar

Rini Asnida Abdullah

Azman Kassim

Norbazlan Mohd Yusof

Norisam Abd Rahaman

Roohollah Kalatehjari